



TEZ ŞABLONU ONAY FORMU
THESIS TEMPLATE CONFIRMATION FORM

1. Şablonda verilen yerleşim ve boşluklar değiştirilmemelidir.
2. Jüri tarihi Başlık Sayfası, İmza Sayfası, Abstract ve Öz'de ilgili yerlere yazılmalıdır.
3. İmza sayfasında jüri üyelerinin unvanları doğru olarak yazılmalıdır.
4. Tezin son sayfasının sayfa numarası Abstract ve Öz'de ilgili yerlere yazılmalıdır.
5. Bütün chapterlar, referanslar, ekler ve CV sağ sayfada başlamalıdır. Bunun için **kesmeler** kullanılmıştır. **Kesmelerin kayması** fazladan boş sayfaların oluşmasına sebep olabilir. Bu gibi durumlarda paragraf (¶) işaretine tıklayarak kesmeleri görünür hale getirin ve yerlerini **kontrol edin**.
6. Figürler ve tablolar kenar boşluklarına taşmamalıdır.
7. Şablonda yorum olarak eklenen uyarılar dikkatle okunmalı ve uygulanmalıdır.
8. Tez yazdırılmadan önce PDF olarak kaydedilmelidir. Şablonda yorum olarak eklenen uyarılar PDF dokümanında yer almamalıdır.
9. **Bu form aracılığıyla oluşturulan PDF dosyası arkalı-önlü baskı alınarak tek bir spiralli cilt haline getirilmelidir.**
10. Spiralli hale getirilen tez taslağınızdaki ilgili alanları imzalandıktan sonra, [Tez Jüri Atama Formu](#) ile birlikte bölüm sekreterliğine teslim edilmelidir.
11. Tez taslağınız bölüm sekreterliğiniz aracılığıyla format ve görünüm açısından kontrol edilmek üzere FBE'ye ulaştırılacaktır.
12. FBE tarafından kontrol işlemleri tamamlanan tez taslakları, öğrencilere teslim edilmek üzere bölüm sekreterliklerine iletilecektir.
13. Tez taslaklarının kontrol işlemleri tamamlandığında, bu durum öğrencilere METU uzantılı öğrenci e-posta adresleri aracılığıyla duyurulacaktır.
14. Tez taslakları bölüm sekreterlikleri tarafından öğrencilere iletileceği için öğrencilerimizin tez taslaklarını enstitümüzden elden alma konusunda ısrarcı olmamaları beklenmektedir.
15. Tez yazım süreci ile ilgili herhangi bir sıkıntı yaşarsanız, [Sıkça Sorulan Sorular \(SSS\)](#) sayfamızı ziyaret ederek yaşadığınız sıkıntıyla ilgili bir çözüm bulabilirsiniz.

1. Do not change the spacing and placement in the template.
2. Write defense date to the related places given on Title page, Approval page, Abstract and Öz.
3. Write the titles of the examining committee members correctly on Approval Page.
4. Write the page number of the last page in the related places given on Abstract and Öz pages.
5. All chapters, references, appendices and CV must be started on the right page. **Section Breaks** were used for this. **Change in the placement** of section breaks can result in extra blank pages. In such cases, make the section breaks visible by clicking paragraph (¶) mark and **check their position**.
6. All figures and tables must be given inside the page. Nothing must appear in the margins.
7. All the warnings given on the comments section through the thesis template must be read and applied.
8. Save your thesis as pdf and Disable all the comments before taking the printout.
9. **Print two-sided the PDF file that you have created through this form and make a single spiral bound.**
10. Once you have signed the relevant fields in your thesis draft that you spiraled, submit it to the department secretary together with your [Thesis Jury Assignment Form](#).
11. Your thesis draft will be delivered to the GSNAS via your department secretary for controlling in terms of format and appearance.
12. The thesis drafts that are controlled by GSNAS, will be sent to the department secretary to be delivered to the students.
13. This will be announced to the students via their METU students e-mail addresses when the control of the thesis drafts has been completed.
14. As the thesis drafts will be delivered to the students by the department secretaries, we are expecting from our students no to insist about getting their theses drafts from the Institute.
15. If you have any problems with the thesis writing process, you may visit our [Frequently Asked Questions \(FAQ\)](#) page and find a solution to your problem.

Yukarıda bulunan tüm maddeleri okudum, anladım ve kabul ediyorum. / I have read, understand and accept all of the items above.

Name : Beyza
Surname : Durusoy
E-Mail : beyza.durusoy@metu.edu.tr
Date :
Signature : _____

DESCRIPTION AND VERIFICATION OF A MODEL TO CALCULATE THE
EFFICIENCY OF A BIFACIAL PV MODULE USING THEORETICAL AND
EXPERIMENTAL OBSERVATIONS

A THESIS SUBMITTED TO
THE GRADUATE SCHOOL OF NATURAL AND APPLIED SCIENCES
OF
MIDDLE EAST TECHNICAL UNIVERSITY

BY

BEYZA DURUSOY

IN PARTIAL FULFILLMENT OF THE REQUIREMENTS
FOR
THE DEGREE OF MASTER OF SCIENCE
IN
PHYSICS

JANUARY 2020

Approval of the thesis:

THESIS TITLE

submitted by **Beyza Durusoy** in partial fulfillment of the requirements for the degree of **Master of Science in Physics, Middle East Technical University** by,

Prof. Dr. Halil Kalıpçılar
Dean, Graduate School of **Natural and Applied Sciences**

Prof. Dr. Altuğ Özpıneci
Head of the Department, **Physics**

Prof. Dr. Bülent Gültekin Akınođlu
Supervisor, **Physics, METU**

Dr. Talat Özden
Co-Supervisor, Energy Systems Eng., **Gümüşhane University**

Examining Committee Members:

Assoc. Prof. Dr. Selami Kesler
Electrical-Electronics Eng., Pamukkale University

Dr. Emre Yüce
Physics, METU

Prof. Dr. Bülent Gültekin Akınođlu
Physics, METU

Date: 17.01.2020

I hereby declare that all information in this document has been obtained and presented in accordance with academic rules and ethical conduct. I also declare that, as required by these rules and conduct, I have fully cited and referenced all material and results that are not original to this work.

Name, Last name : Beyza Durusoy

Signature :

ABSTRACT

DESCRIPTION AND VERIFICATION OF A MODEL TO CALCULATE THE EFFICIENCY OF A BIFACIAL PV MODULE USING THEORETICAL AND EXPERIMENTAL OBSERVATIONS

Durusoy, Beyza
Master of Science, Physics
Supervisor : Prof. Dr. Bülent Gültekin Akınoğlu
Co-Supervisor: Dr. Talat Özden

January 2020, 55 pages

Bifacial solar modules can use the solar irradiation reaching directly to its back surface as their cells are constructed to have photovoltaic response for both faces. They have been investigating since 1960s and hold a promising future compared to mono-facial cells. Since bifacial solar modules capture photons from both surfaces, the efficiency of a bifacial solar module strongly depends on the rear side illumination. This thesis aims to construct a model to calculate the rear side solar irradiation incident on a bifacial module. We also examine the variation of solar irradiation at different heights of the rear surface and effect of shading. The thesis also aims to outline a model procedure to reach the yield of a bifacial module. The modelling is verified using experimental data measured in GÜNAM's Outdoor Test Facility.

Keywords: Solar Energy, Bifacial PV, Modelling PV, Renewable Energy, Energy Technologies

ÖZ

DENEYSEL GÖZLEMLERİ KULLANARAK ÇİFT TARAFLI FOTOVOLTAİK MODÜLÜN VERİMLİLİĞİNİ HESAPLAMAK İÇİN BİR MODELİN BETİMLENMESİ VE DOĞRULANMASI

Durusoy, Beyza
Yüksek Lisans, Fizik
Tez Yöneticisi: Prof. Dr. Bülent Gültekin Akınoğlu
Ortak Tez Yöneticisi: Dr. Talat Özden

Ocak 2020, 55 sayfa

Çift taraflı güneş modülleri, iki yüzeyi de fotovoltaik tepki verecek şekilde yapılandırıldığı için arka yüzeyine ulaşan güneş ışınlarını kullanabilir. 1960lardan beri araştırılmakta olan bu tür paneller gelecek vaat etmektedir. Çift taraflı güneş panelleri, ön ve arka yüzeyine doğrudan güneşten gelen ve yerden yansıma sonucu panele ulaşan güneş ışınlarını yakaladığı için; arka yüzeyine gelen güneş ışını miktarı, modülün verimliliği için oldukça önemlidir. Bu tezin amacı, çift taraflı güneş panellerinin arka yüzeyine ulaşan güneş ışını miktarının modülün yerden yüksekliğine bağlı değişimlerinin incelenmesidir. Tez ayrıca, çift taraflı bir modülün verimliliğine ulaşmak için bir modelin ana hatlarını çizmeyi amaçlamaktadır. Model, deneysel bulgular kullanılarak ayarlanacak ve doğrulanacaktır.

Anahtar Kelimeler: Güneş Enerjisi, Çift Taraflı FV Modülleri, FV Modellemesi, Yenilenebilir Enerji, Enerji Teknolojileri

To the buoyancy of life

ACKNOWLEDGMENTS

I would first like to thank my thesis advisor Prof. Dr. Bülent G. Akınođlu, of the Department of Physics at METU. He was always there for me when I needed help with my research or academic life in general. He allowed this study to be my work but steered me in the right direction when needed. He taught me not only physics but also so many life lessons. I could not have imagined having a better advisor and mentor for my MSc. study.

I would also like to thank my co-advisor, Asst. Prof. Dr. Talat Özden for his consistent support and guidance. He always enlightens me with straightforward suggestions. Without his contribution, especially in the last weeks, this study would be incomplete.

I acknowledge the support given by the Ministry of Development for the construction of the outdoor testing facility. Project number: BAP-08.11.2015K121200, 2015 – 2019. Moreover, I would like to thank GÜNAM for the use of the outdoor facility.

I would like to thank M. Hakan Akınođu for all the support he provided for some of the drawings in this study. I would also like to thank all my MSc. colleagues, especially Seçil Güler, with whom I have shared moments of deep anxiety during this period. Special thanks to Merve Yüksek and Begüm Kaya for bringing positivity to my life. I am also very grateful to İpek Akın and Aline Latus for showing me the distance is nothing when someone means everything.

I also want to thank my partner, Berk Nezir Gün, for his endless support and unconditional love. Thank you for keeping things going and for always showing how proud you are of me.

Finally, I must express my very profound gratitude to my parents and especially to my dear sis, Betül Durusoy, for providing me with unfailing support and continuous encouragement through the process of writing this thesis. Sorry for being even grumpier than usual while writing this thesis! Thank you.

TABLE OF CONTENTS

ABSTRACT.....	v
ÖZ.....	vi
ACKNOWLEDGMENTS.....	vii
TABLE OF CONTENTS.....	ix
LIST OF TABLES.....	xi
LIST OF FIGURES.....	xii
1 INTRODUCTION.....	1
1.1 Solar Energy.....	2
1.2 Bifacial Photovoltaics.....	6
1.3 Thesis Motivation.....	10
2 MODELLING.....	13
2.1 Solar Geometry.....	13
2.2 Components of Solar Irradiation.....	15
2.3 Rear Side Irradiation Calculation.....	19
2.4 PV Yield Calculation.....	24
2.5 Bifacial Yield Modelling.....	26
3 OUTDOOR TESTING SITE AND MEASUREMENTS.....	29
3.1 Test Site and the Module.....	29
3.2 Measurement System.....	30
3.2.1 Environmental Measurements.....	31
3.2.2 PV Module and Measurement Configurations.....	32
3.3 Verification Methods.....	33

4	RESULTS AND DISCUSSION.....	35
4.1	Solar Irradiation.....	35
4.2	Bifacial PV Yield	42
5	CONCLUSION	45
5.1	Future improvements.....	46
	REFERENCES	49

LIST OF TABLES

TABLES

Table 2.1 $R_{b,back}$ calculation between sunrise and sunset for an arbitrary day.	22
Table 2.2 The set of system parameters that are required for PVWatts calculator is listed below for our configuration.....	27
Table 3.1 Summary of the geographical information of the test location.	29
Table 3.2. Summary of the parameters that the test device measures for the performance assessment of PV modules.....	31
Table 3.3. Summary of the properties of the bifacial PV module	32
Table 4.1. Results of statistical error calculations by using three different methods for each configuration	41
Table 4.2. Results of statistical error calculations for bifacial PV yield by using three different methods for each configuration for two different days.....	43

LIST OF FIGURES

FIGURES

Figure 1.1. A comparison of monofacial and bifacial cells and modules.	7
Figure 2.1. Representation of solar angles.	15
Figure 2.2. Components of solar irradiation incident on a bifacial PV module.....	18
Figure 2.3. A representation of the Sun’s path during summer. Here, green arrows indicate the radiation incident on the front surface between the hours 08:00 and 18:00, and red arrows imply that the Sun is behind the surface and there is beam contribution of the sunlight on the rear surface during the sunrise and the sunset. Blue arrows show the ground reflected radiation on the rear surface.	21
Figure 2.4. A sequence of a bifacial PV yield modelling.....	28
Figure 3.1. (a) Outdoor Test Facility in GUNAM, METU. The tested bifacial module is indicated by the red rectangle. (b) Representation of all components in the test facility.	30
Figure 3.2 Test site and the cabin of multi tracer	30
Figure 3.3. Meteorological Station (Davis Vantage Pro2+) and sensors (Kipp&Zonen CMP11).....	32
Figure 3.4 (a) First configuration with one pyranometer is at the bottom-back (0.50 m) and the other is at the middle-back (0.84m). b) Second configuration with one pyranometer is at the top-back (1.16 m) and the other is at the middle-back (0.84 m) c) Third configuration with one pyranometer is at the bottom-back (0.50 m) and the other is at the top-back (1.16 m).....	33
Figure 4.1. Horizontal irradiance measurements simultaneously with rear side irradiance measurements for (a) first configuration (b) second configuration (c) third configuration	36
Figure 4.2 Rear side irradiance measurements for (a) first configuration (b) second configuration (c) third configuration	37
Figure 4.3. Rear side irradiances compiled like a one day for three elevations (a) For a cloudy day, 19 June 2019 (b) For a clear day, 20 June 2019	38

Figure 4.4. The shading path on a partially cloudy day	39
Figure 4.5. Measured and estimated rear side irradiances for (a) first configuration (b) second configuration (c) third configuration.....	40
Figure 4.6. Measured and estimated DC power output for (a) first configuration (b) second configuration (c) third configuration	43
Figure 4.7. Monthly estimated and measured energy yield of a bifacial PV yield over a year.....	44

CHAPTER 1

INTRODUCTION

Since the very beginning of civilizations, people seek energy resources to sustain all their needs. It had been started with wood and coal and continues with electrical energy. Although the requirement of energy is identical to early and modern societies, the population varies significantly. The population of the World has been increasing faster and faster, and at one point, it will no longer be able to meet the energy demands (Nakicenovic & Jefferson, 1996) since the most used energy resources such as coal and natural gas are limited. Besides, fossil fuel-based energy production increases greenhouse gas emissions, which causes climate change (Höök & Tang, 2013). These lead to the transition in the energy sector, and renewable energy resources have gained importance.

Within the acknowledgment of the fact that climate change is a global concern and every country should take action, "The Kyoto Protocol to the United Nations Framework Convention on Climate Change" had been arranged. There are 192 parties to the Kyoto Protocol to the UNFCCC, which accepted reducing their overall greenhouse gas emissions by at least 5 percent below 1990 levels until 2012 (United Nations Framework Convention on Climate Change (UNFCCC), 1998). After the commitment period, the decision had been made for devising a new global agreement, Paris Agreement (2015), to reduce greenhouse gas emissions. This agreement aims to limit the global temperature to below 2 °C by 2030 (UNFCCC, 2015). Letting the output of these agreements aside, the Kyoto Protocol and its predecessor, the Paris Agreement, have become a significant step for attendant countries towards climate change and the transition to renewable energy.

The term 'renewable' refers to the energy resources that are replenished at the same rate as they are 'used' (Armstrong & Hamrin, 2000). Primary renewable energy resources are wind power, solar power, hydropower, and biomass (Bilgen, Kaygusuz, & Sari, 2004; Dincer, 2001). Wind, wave, hydro and biofuels are the indirect use of Sun's energy, which then makes the solar energy is the leading renewable energy resource (Freris & Infield, 2009, pp. 14–15). According to the Renewables 2019 Global Status Report, the renewable energy share in electricity generation was around 26% by the end of 2018. Now, net capacity additions for renewable power is more than one-third of total capacity. As of 2017, modern renewables (excluding nuclear energy and traditional biomass) supplied 10.6% of total final consumption. The most significant contribution comes from thermal energy ($\cong 4.2\%$), followed by hydropower (3.6%) and other sources such as hydropower, solar power, biomass (2%), and transport biofuels ($\cong 1\%$). The remaining part of the renewable energy share still relies on traditional biomass since wood is mostly used for heat and cooking in developing countries (REN 21 Renewables Now, 2019, pp. 29–31).

Although the share of the direct use of solar energy is mediocre compared to hydropower, and hydropower is a substantial resource, but it is widely dependent on the location; therefore, its contribution is not comparable to other sources. Moreover, investments on large-scale solar project has been increasing rapidly. For example, the International Solar Alliance (ISA) 's objective of investment is USD 1 trillion by 2030 for the deployment of solar energy (REN 21 Renewables Now, 2019, p. 31).

1.1 Solar Energy

Without mentioning the main properties of the Sun, the concept of photovoltaic or other systems that convert solar energy into useful energy, would not be completed. The Sun is a sphere of intensely hot gaseous matter with a diameter of 1.39×10^9 m and is, on the average of 1.5×10^{11} m from the Earth. The Sun has an effective blackbody temperature of 5777 K, and it radiates energy at the rate of 3.9×10^{26} W.

Several fusion reactions are occurring inside of the Sun to provide this energy. The most critical process is that hydrogen (four protons) combines to form the helium, and energy is released because the helium nucleus has less energy than the original four protons. The energy produced in the core of the Sun transfers out to the surface and then radiates into space. Due to the eccentricity of the Earth, the distance between Earth and Sun varies by 1.7 %, but at the mean Sun-Earth distance, the radiation emitted by the Sun is nearly fixed. The Solar constant $G_{sc} = 1367 \pm 2 \text{ W/m}^2$ is the extraterrestrial radiation from the Sun on a unit area of the surface perpendicular to the direction of the radiation at the mean Sun-Earth distance (Duffie, Beckman, & McGowan, 1985, p. 5). The amount of solar energy that reaches the Earth in one hour can meet the energy demand of the World for one day (Masters, 2013, p. 445). However, converting solar energy into useful energy is a rather complicated process and collected by two different technologies: solar thermal and photovoltaics (PV).

Solar thermal systems are based on the principle of heating the fluid (water or other) and fed it into the radiator system. The most common type of solar thermal system is of the thermosyphon type, which consists of two flat plate collectors with a storage tank (Kalogirou, 2014, p. 239). The collector absorbs sunlight and, the water inside is heated up. As the medium inside the solar collector is heated, the hot fluid starts to rise by pushing the cold fluid down in the storage tank to repeat the cycle. Due to the pressure difference between the hot liquid and cold liquid, there is no need for a mechanical pump. This type of system is called ‘passive systems’ and mainly used for hot water or house heating. Active solar thermal systems consist of collectors, a distribution system, and a storage component (Kalogirou, 2014, p. 271). With the use of the mechanical pump, the cold fluid drawn to the flat plate collector absorbs the energy and returns to the tank. The hot fluid is either transferred into a room by heating coils or to a storage system.

The term photovoltaic (PV) refers to the direct conversion of sunlight into electricity. A PV cell system consists of a layer or more semiconductor material when exposed to a photon with high enough energy, an electron in the PV material can break free

of the atom that it holds. This electron is carried away by contacts as a current. Multiple cells are connected and covered by a glass-like material to construct a PV module (or panel) (Antonio Luque & Hegedus, 2011, pp. 4–7). One of the advantages of PV systems, PV cells, and indeed, modules can be connected to reach the desired power output. Most PV systems generate direct current; on the contrary, most household tools use alternating current; therefore, an inverter is a must-have component of these systems. Apart from the inverter, batteries, and a collection of PV modules, namely, a PV array, are essential for constructing a functional PV system. There are two main categories of PV systems: grid-connected and stand-alone PV systems. Grid-connected systems connected to the local electricity network (grid), whereas stand-alone systems are independent of the grid supply.

Photovoltaic modules are solid-state devices; therefore, a piece of general knowledge on semiconductors is needed. An atom consists of nucleus and electrons that orbit the nucleus. Quantum mechanics states that an isolated atom can only have discrete or quantized energy levels (Kalogirou, 2014, p. 483) If two or more atoms brought together, their energy levels are unified in energy bands. Electrons in the outermost shell have less energy than the ones that are strictly attached to the nucleus. For this reason, it is easier for atoms in the outermost shell to interact with the nearby atoms (Goswami, 2015). This energy band corresponds to the ground state of valance electrons in an atom, and that is why it is called valance band. When loosely attached electrons in the valance band interact, and attach with the nearby atom, that leaves the original atom as a positive ion. They can also have enough energy to jump into a higher energy band, which is the conduction band. In this way, they conduct electricity or heat. The energy difference between the conduction and the valance band is called the bandgap (Fiore, 2018).

If the valance band is full and the conduction band is empty, the bandgap between these bands would be very high, and this type of material are called insulators. Overcoming the bandgap is rather tricky, and therefore no current can be conducted (Pierret, 1996). On the contrary, when the valance band is relatively empty, and the conduction band is partially full of some electrons, electrons can accept energy from

an external field. With the help of external field, they can move to the conduction band. In this type of materials, namely conductors, valance band and conduction band overlaps since the bandgap is significantly small. Metals are conductors, and electrons in valance band in a metal can quickly become free and conduct current. Materials with partially filled valance band and narrower band gaps than insulators are called semiconductors. There are two types of semiconductors: intrinsic and extrinsic semiconductors. Intrinsic ones are pure semiconductors, whereas extrinsic ones are doped with some impurities. Electrons in the valance band of a semiconductor can jump to the conduction band with external energy, and this is because the bandgap is relatively narrow (Goswami, 2015).

When a semiconductor is doped with a material that has more electrons in its valance band than the semiconductor, the doped material is called n-type semiconductor. Although the material is electrically neutral, it appears as if there are excess electrons that are available for conduction. For example, if silicon is doped with phosphorus atom, the doped silicon is called n-type since phosphorus has one more electron in its valance band than the silicon. On the other hand, boron has three electrons in its valance band, which is one less electron than the silicon, and if silicon is doped with boron, it seems like there is one missing electron, namely, a positive hole. This type of material is called p-type materials. If p and n-type material are brought together, they form a junction. Excess electrons in the n-type side move to the p-type side to fill the holes and the holes from the p-type side diffuse to the n-type side. In this way, the n-type side close to the junction becomes positively charged, and the p-type side negatively charged. The negative charges in the p-type side prevent the movement of additional electrons from the n-type side, but holes in the n-type side enable additional electrons in the p-type side to move to the n-type, which makes the semiconductor behave like a diode (Neamen, 2006).

When a photon is absorbed by the valance electron, the energy of the photon is transferred to the electron, and if this energy is less than the bandgap, then the excess energy of electrons causes an increase of the temperature, and no electron can be removed from the atom. Unless the electron jumps to the conduction band, and this

electron can be freed by an electric field due to the p-n junction, thus creating a current. Without the E-field, this electron recombines with the atom and no current flows. The important thing is that only one electron can be freed, independent of the intensity of the photon energy, which is the main reason for the low conversion efficiency of solar cells (Bhattacharya & John, 2019).

As the sunlight strikes to the surface of the solar cell, free electrons are generated in the n-side, and these electrons combine with holes creating electron-hole pairs. When these pairs are near to the p-n junction, E-field between the sides separates them in a way that electrons move to the n-side and holes to the p-side. By connecting two sides of the solar cell through a load, forming an electrical circuit, the current, namely photocurrent (I_{ph}), can flow when the sunlight strikes. During the night time, no current is generated, but if there is an external voltage supply connected to the p-n junction, then it generates diode or dark current (I_d). The net current is the difference between the photocurrent and the dark current. A solar cell, module or an array can be represented by an electrical one-diode model which consists of a current source, diode, series and shunt resistances (Kalogirou, 2014, pp. 488–495).

1.2 Bifacial Photovoltaics

Bifacial solar cells are designed to convert sunlight that strikes the surface of the solar cell from both the front and rear sides. There are only a few but complicated steps in the fabrication process of bifacial solar cells when compared to monofacial solar cells (Saw, Khoo, Singh, & Wang, 2017; Van Aken, Okel, Liu, Luxembourg, & van Roosmalen, 2016). During the fabrication of monofacial solar cells, the metal contacts are screen printed by using a silver paste for the front side and by using aluminum paste for the rear side. Because of this metallization process, the rear side of monofacial cells are fully covered, and they are unable to convert rear side illumination into electricity (A. Luque, Ruiz, Cuevas, Eguren, & Gomez-Agost, 1980). When bifacial cells are connected and covered by a glass-like material, they form a bifacial PV module. Figure 1.1 shows a comparison of monofacial and

bifacial cells and modules. Since bifacial PV modules can capture the rear side illumination in addition to the front side, they have higher efficiency than monofacial PV modules. The efficiency of bifacial PV depends not only on the properties of the cells themselves but also on mounting conditions (Guo, Walsh, & Peters, 2013).

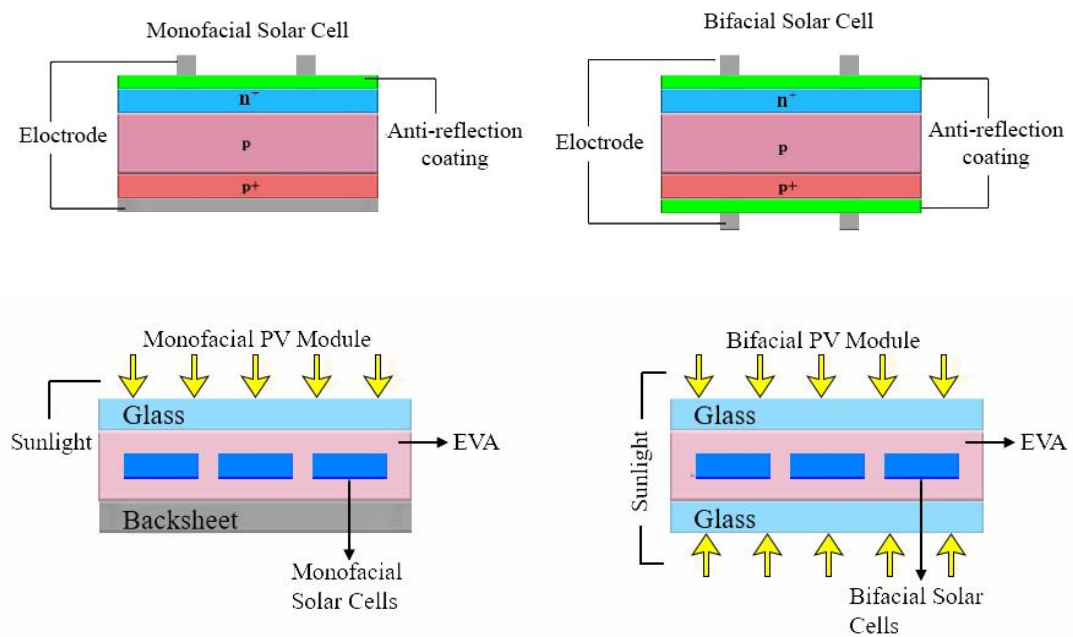


Figure 1.1. A comparison of monofacial and bifacial cells and modules.

In 1960, H. Mori fabricated the first bifacial solar cells by forming a p^+np^+ structure on both surfaces (Patent No. 3.278.811, 1966). The starting point of the production was to increase the collection efficiency for long-wavelength photons and to improve the surface passivation (“Bifacial Photovoltaics Technol. Appl. Econ.,” 2018, p. 19) The first transistor-like (p^+np^+/n^+np^+) bifacial devices are proposed by the research group at the UPMadrid in Spain, and the conversion efficiency of these devices reached 7% (A. Luque et al., 1980). There were many studies conducted on the fabrication of bifacial cells so that the conversion efficiency of the bifacial solar cells increased from 7% to above 20% by the year 1980 (Cuevas, Luge, & Ruiz, 1980). Moreover, bifacial solar cells were also used in space applications since they are able to capture solar irradiation reflected from the Earth (Meulenber, Allison, & Arndt,

n.d.; Strobl, Kasper, Rasch, & Roy, 1985). According to findings of the experiments that are conducted in the first space station program of the Soviet Union, the contribution of the rear side irradiance was on the level 10-20% depending on the orientation (Letin, Kagan, Nadorov, & Zajavlin, 2000).

The additional rear side irradiance strongly depends on the albedo (ground-reflectance). To compare a flat panel with bifacial BSF solar cell, measurements had been made in a site which has remarkably high ground reflectance. The result was that bifacial panel produces 42-63% more power than the flat panel (Cuevas, Luque, Eguren, & del Alamo, 1982).

A ratio between the rear and front responses of the device is needed to analyze the bifacial performance of the model. This ratio is called the bifaciality factor, which determines the additional energy yield of the rear side (Kopecek et al., 2015). The bifaciality factor can be expressed for nominal efficiency, power, short circuit current density, and open-circuit voltage and often denotes as a percentage (“Bifacial Photovoltaics Technol. Appl. Econ.,” 2018, p. 22)

Although the bifaciality factor is an important parameter to estimate the rear side output power, real-life conditions significantly vary with standard test conditions. Module installation conditions, environment, the distance between the modules, shadowing effects, and the albedo of the ground have a significant effect on the additional energy yield of the bifacial PV module (Wang et al., 2015a). For this reason, it is rather difficult to describe a model to calculate the energy yield of bifacial modules than monofacial modules.

There are many studies on modelling the rear side irradiance of bifacial PV modules with the use of the view factor approach. In the article of Modelling of bifacial gain for stand-alone and in-field installed bifacial PV modules, two view factors are calculated to estimate the rear side irradiance of the bifacial module: one for the shadowed region to the module and the other for the area outside the shadow to the module. Since the shadow is continuously moving, the calculation of the view factor repeated every 15 mins for each cell of the module individually (Shoukry, Libal,

Kopecek, Wefringhaus, & Werner, 2016). Instead of calculating the view factor for each cell of the module, a practical irradiance model for bifacial PV modules has been proposed. The model calculates the rear side irradiance for each row of cells, and by doing so, the rear side irradiance differences along the rows remain ignored. However, this simplification makes the computation process much easier (Marion et al., 2018). Another attempt at modelling the additional energy yield of bifacial modules is made by (Ufuk Alper Yusufoglu et al., 2014). The view factor method is used to calculate the rear side irradiance of south-facing bifacial PV modules. In this study, simulations are done for a single module to optimize the installation conditions, such as the elevation of the module and the tilt angle (Ufuk Alper Yusufoglu et al., 2014). The use of view factors implemented by (Janssen, Van Aken, Carr, & Mewe, 2015) differently. Unlike other models that are presented above, the anisotropic sky approach is used for calculating the front and rear side irradiances. These calculated irradiances are taken as inputs for the proposed thermal model and electrical models (Janssen et al., 2015).

Another approach is the ray-tracing method, which is based on the tracking of sunlight's beam by using the Monte Carlo approach. The use of ray-tracing is to calculate the interaction between objects and light sources. Besides, reflection and refraction paths of the beam can be traced as well (Louw & Rix, 2019). Ray-tracing implementations for estimating the rear side irradiance of bifacial PV modules have usually been done by using commercialized software. For example, in the article "A sensitivity study of the impact of installation parameters and system configuration on the performance of bifacial PV arrays", a utilized RADIANCE software-based ray-tracing model has been used to analyze the effect of installation parameters on the bifacial gain. One drawback of RADIANCE is that only three wavelengths can be simulated at a time; therefore, the procedure must be repeated until the full spectrum is achieved (Lo, Lim, & Rahman, 2015). The modeling of multiple module configurations has been done, but only the middle module in each array is considered to make the analysis feasible (Asgharzadeh, Marion, et al., 2018). Another use of the ray-tracing approach is to predict the annual energy yield by bifacial PV modules

with short-term data. This has been done by creating a simple optical model for a test bench, and with this model, hourly irradiance on the backside can be simulated. In this study, real-life conditions, solar geometry, and reflective losses are ignored (Soria, Gerritsen, Lefillastre, & Broquin, 2016).

An analysis of irradiance models for bifacial PV modules has been done in the National Renewable Energy Laboratory (NREL). View factor models for bifacial PV cells and arrays, and ray-tracing models using the RADIANCE and COMSOL software packages have been used. Simulation results and measured data are compared. Both results are in agreement with data. Although ray tracing simulations give more a detailed outlook of features in the module and array design, they are not practical to use due to the computational requirements. View factor simulations at the cell level are suitable for small arrays, but it could be time-consuming to implement on larger arrays (Hansen et al., 2017)

1.3 Thesis Motivation

The purpose of this thesis is to describe a model for calculating the efficiency of a bifacial PV module and verifying the model by using experimental observations. The model introduced here does not require high computational power, and it can be adjusted for different geometries and installation conditions. Detailed analysis of bifacial PV module performance was presented concerning the elevation factors. Moreover, a comparison is being carried out between bifacial and monofacial PV performance with the help of simulations

In the next section, solar angles and components of solar irradiation were introduced to calculate the rear side irradiation. Input and output data and the flow of the scheme were outlined to compose a PV model. In the third section, a brief information of the test site and measurement system is given. The focus of the fourth chapter is on the results of the study, which include the rear side irradiation calculation for three configurations and the energy yield simulations. The proposed model and

simulations were verified by using outdoor measurements. The effect of the elevation on the additional rear side irradiation incident on the bifacial PV performance were analyzed. In the last chapter, the conclusion of the study and further improvements were discussed.

To sum up, for analyzing the performance of bifacial PV parameters, a model was proposed and verified by using outdoor measurements. Factors that have the effect on the rear side irradiation and the energy yield of the bifacial PV module were examined.

CHAPTER 2

MODELLING

2.1 Solar Geometry

To obtain a relationship between the position of the module and the incoming beam radiation, a unified definition of angles is needed. The set of such angles is defined by (Benford and Bock,1939) and they can be used for two different purposes: (1) To estimate the orientation of the Sun at a given time and (2) to classify the orientation and mounting conditions of the PV module. Figure 2.1. includes some of the solar angles that are used in this study.

(1) Estimation of Sun's position

Declination angle (δ): The Earth's orbit around the sun is elliptic meaning that Earth's axis is inclined 23.45° relative to the plane of Earth's path around the Sun. Therefore, Sun rays come from different directions relative to equatorial plane. This is known as the declination (δ), i.e. the angle between the direction of the Sun rays and the equatorial plane ($-23.45^\circ \leq \delta \leq 23.45^\circ$).

Declination can be found by the following formula (Cooper, 1969)

$$\delta = 23.45^\circ \sin \left[\frac{360}{365} (n + 284) \right] \quad (1)$$

where n is the ith day of the year.

Or more accurately as stated by (Spencer, 1971, p. 172)

$$\delta = \left(\frac{180}{\pi} \right) (0.006918 - 0.399912 * \cos(B) + 0.070257 * \sin(B) - 0.006758 * \cos(2B) + 0.000907 * \sin(2B) - 0.002697 * \cos(3B) + 0.00148 * \sin(3B)) \quad (2)$$

where B is an empirical constant and it can be determined from

$$B = (n - 1) * \frac{360}{365} \quad (3)$$

Hour angle (ω): Earth rotates around its axis (360°) every 24 hours, i.e., 15° each hour. Hour angle is defined as the angular displacement of the Sun east or west of the local meridian. At solar noon, the hour angle is accepted as 0° , before noon is taken as negative and the afternoon positive. For example; at 11:00, hour angle is -15° and at 13:00, it is $+15^\circ$. (Solar time is taken account)

Zenith angle (θ_z): The angle between the vertical and the solar beam

$$\cos\theta_z = \cos\phi\cos\delta\cos\omega + \sin\phi\sin\delta \quad (4)$$

Solar altitude angle (α_s): The angle between the horizontal and the solar beam. Solar altitude and zenith are complementary angles, i.e., $\alpha_s + \theta_z = 90^\circ$

Solar azimuth angle (γ_s): The angle of Sun's beam measured in the horizontal plane from true south (For the Northern hemisphere) . (0° for south, 180° for north facing surfaces)

(2) Classification of the orientation of the PV module

Latitude (Φ): The angular position of the north or south of the equator

Slope or tilt angle (β): The angle between the plane of the module and the horizontal.

Surface azimuth angle (γ): The angle between the normal to horizontal and the local meridian.

Angle of incidence (θ): The angle between the solar beam on a surface and the normal of that surface.

$$\cos\theta = \sin\delta\sin\phi\cos\beta - \sin\delta\cos\phi\sin\beta\cos\gamma + \cos\delta\cos\phi\cos\beta\cos\omega + \cos\delta\sin\phi\sin\beta\cos\gamma\cos\omega + \cos\delta\sin\beta\sin\gamma\sin\omega \quad (5)$$

If the angle of incidence is greater than 90° , the sun rays reach to behind the surface (Duffie et al., 1985, p. 14). A short period of time of the year (during summer), the

angle θ , exceeds 90° . Therefore, sun rays impingin on the rear surface contributes to the additional yield of bifacial PV modules since the rear side illumination is captured as well.

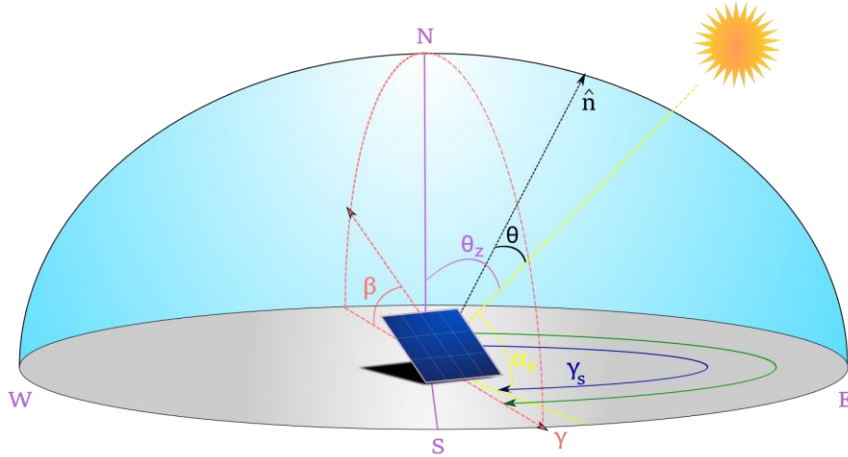


Figure 2.1. Representation of solar angles.

2.2 Components of Solar Irradiation

Solar irradiation is the energy delivered by the Sun to the Earth by means of electromagnetic radiation. For solar energy applications or PV modelling purposes, a portion of the electromagnetic radiation in a wavelength range of 0.25 to $3.0 \mu\text{m}$ (known as solar spectrum) is taken account (Wasfi, 2011). The radiation that would be received without the atmosphere is called extraterrestrial radiation and can be found by (Spencer, 1971):

$$G_{on} = G_{sc} \left(1 + 0.033 \cos \frac{360n}{365} \right) \quad (6)$$

Or more accurately, with $\pm 0.01\%$ error (Iqbal, 1983) :

$$G_{on} = G_{sc} (1.000110 + 0.034221 \cos B + 0.001280 \sin B + 0.000719 \cos 2B + 0.000077 \sin 2B) \quad (7)$$

where G_{on} is the extraterrestrial radiation imping on a surface normal to the radiation, n is the day number, and B is a constant that depends on n . (3). The variation of the extraterrestrial radiation is mainly because of the variation in the emitted radiation and the changing earth-sun distance.

Within the atmosphere, the solar radiation components can be divided into two main groups; the direct (beam) and the diffuse solar radiation. Sum of these two components refers to the term global solar radiation.

Beam (direct) radiation is the solar radiation received from the Sun without scattering by the atmosphere.

Diffuse radiation is the solar radiation received from the sun after scattering by the particles in the atmosphere such as dust or aerosols (Duffie et al., 1985, p. 10).

To calculate the total radiation on a tilted surface, direction of the beam and diffuse radiation components are needed. Coulson (1972) proposed a diffused radiation model which composed of three parts. The first is an isotropic part, meaning that radiation distributes uniformly from the entire sky dome. The second is circumsolar diffuse caused by the forward scattering of solar radiation. The last part is the horizon brightening, as the name suggests, it is concentrated near the horizon.

The proposed model is a mathematical representation of the diffuse radiation and together with the beam and reflected radiation, total radiation on a tilted surface can be calculated if only horizontal radiation is known from measurement.

$$I_t = I_{t,beam} + I_{t,diffuse} + I_{t,reflected} \quad (8)$$

and

$$I_{t,diffuse} = I_{t,hz} + I_{t,cs} + I_{t,iso} \quad (9)$$

A total incident radiation on a tilted collector with an area of A_c can be found as follows

$$A_c I_t = I_b R_b A_c + I_{d,iso} A_s F_{s-c} + I_{d,cs} R_b A_c + I_{d,hz} A_{hz} F_{hz-c} + \sum_i I_i \rho_i A_i F_{i-c} \quad (10)$$

The first component refers to the beam part of the radiation. The second component is the isotropic part of the diffuse radiation with an unknown sky area A_s and the radiation view factor from sky to the collector. The third is the circumsolar diffuse. The fourth part is the diffuse from the horizon from an unknown area A_{hz} and the view factor from horizon to the collector F_{hz-c} . The last part of the equation presents the sum of each reflected streams from the ground and surroundings. I is the solar radiation, ρ is the albedo and the F_{i-c} is the view factor from the i th surface to the collector. Since reflected radiation part is extremely complex and it is not possible to calculate, the above equation can be simplified as follows (Duffie et al., 1985, pp. 86–87)

$$I_t = I_b R_b + I_{d,iso} F_{c-s} + I_{d,cs} R_b + I_{d,hz} F_{c-hz} + I \rho_g F_{g-c} \quad (11)$$

Here, it is assumed that there is only one horizontal reflecting ground surface, then the sum drops off as well. The reflectance coefficient, i.e., the albedo of the ground and the view factor from the ground to the collector have been taken. To get rid of undefined areas, view factor reciprocity relations; $A_s F_{s-c} = A_c F_{c-s}$ & $A_{hz} F_{hz-c} = A_c F_{c-hz}$ are used. These relations cancel all the area elements in the above equation. However, there is still a parameter remaining undetermined, R_b which is the ratio of beam radiation to the total radiation. There are several approaches for calculating R_b but the following method (Duffie et al., 1985, p. 88) is used in the scope of this thesis:

$$R_b = \frac{\cos\theta}{\cos\theta_z} \quad (12)$$

However, the ratio of beam radiation changes rapidly for the sunrise and sunset hour, and for these hours R_b can be calculated as follows:

$$R_{b,ave} = \frac{a}{b} \quad (13)$$

$$a = (\sin\delta\sin\phi\cos\beta - \sin\delta\cos\phi\sin\beta\cos\gamma) \frac{1}{180} (\omega_2 - \omega_1)\pi + (\cos\delta\cos\phi\cos\beta + \cos\delta\sin\phi\sin\beta\cos\gamma)(\sin\omega_2 - \sin\omega_1) - (\cos\delta\sin\beta\sin\gamma)(\cos\omega_2 - \cos\omega_1)$$

and

$$b = (\cos\phi\cos\delta)(\sin\omega_2 - \sin\omega_1) + (\sin\phi\sin\delta)\frac{1}{180}(\omega_2 - \omega_1)$$

Apart from the diffuse radiation model, one common sky model is the isotropic diffuse model derived by Liu and Jordan (1963). It is based on the assumption that all diffuse radiation is isotropic, meaning that the radiation on a tilted surface composed of three components; beam, isotropic diffuse and diffusely reflected from the ground. This simplifies the Equation 11, and the radiation on a tilted surface can be written as follows:

$$I_t = I_b R_b + I_d \left(\frac{1+\cos\beta}{2}\right) + I\rho_g \left(\frac{1-\cos\beta}{2}\right) \quad (14)$$

Here, $\left(\frac{1+\cos\beta}{2}\right)$ represents the view factor from collector to the sky and $\left(\frac{1-\cos\beta}{2}\right)$ the view factor from the ground to the collector.

Figure 2.2 shows the modified version of isotropic sky model which includes the rear side irradiation impinging on a bifacial PV module.

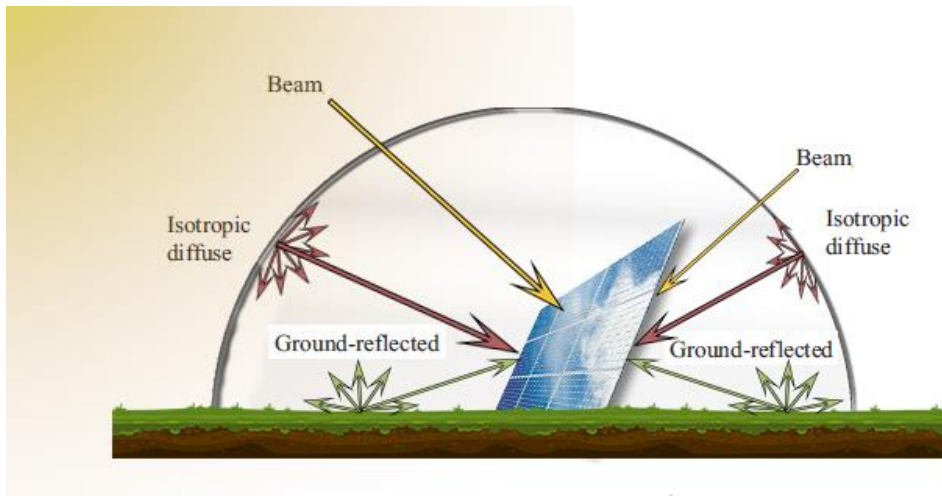


Figure 2.2. Components of solar irradiation incident on a bifacial PV module.

2.3 Rear Side Irradiation Calculation

A bifacial cell captures rear side irradiation as its rear side is not coated in a way that prevents light passing through. The major difference between the monofacial and the bifacial cell is the rear side irradiation. For this reason, it is important to estimate the rear side irradiation to make feasibility studies of bifacial PV modules. Up to now, there are a few feature attempts of the commercialized software programs such as PVYSYST and SAM, but their features currently underestimate the additional energy gain of bifacial PV modules (Photovoltaik-Institut Berlin PI, 2019). The problem in the market is that there is no commercial simulation software program or a modelling approach to assess the field performance of bifacial PV modules.

For the estimation of the rear side irradiation, we have used a similar approach to that of Liu and Jordan's isotropic sky model and we have done three modifications to that model.

First modification: Tilt Angle

The tilt angle is defined as the angle between the ground and the module. To define an optimal tilt angle for a PV system is somewhat tricky since the tilt angle is highly dependent on the location. Besides, the elevation of the module and the albedo affect the tilt angle as well. Although it is previously stated that when the tilt angle equals to the latitude, then, the energy yield of bifacial PV modules gets maximum (D.Faiman & A.Dolev, 2004), other parameters such as the elevation and the albedo should be considered together for performance analysis of bifacial PV modules. For example, while a smaller tilt angle is the optimum for high albedo ($\alpha = 0.5$) at 0.5m elevation, it increases sharply with the increasing elevation ($h = 1\text{ m}$). Another point is that decreasing the tilt angle increases the uniformity of the rear side solar irradiation since the height difference between the lower and upper edges of the module reduces with the decreasing angle (Ufuk A. Yusufoglu et al., 2015). Since many parameters affect the performance of the bifacial PV module, there is no standardized method for determining the optimal tilt angle.

Although bifacial PV modules with optimal installation conditions will produce more energy, our test facility and mounting of the tested module do not necessarily have optimal conditions. The tilt angle is fixed to 32, the height of the module from the ground is 0.5 m, and the reflectance of the ground is rather a low value of 0.2. It is also crucial to conduct performance analysis of PV modules in real life, considering all non-ideal conditions since life is not ideal after all.

In the northern hemisphere, for a south-facing PV module at a tilt β° , the solar irradiation incident on that module can be found by using Equation (14) as stated in the previous section. The first alteration is the tilt angle for finding the solar irradiation incident on the rear surface of that module. Instead of β , the complementary of β is used since the rear side is at a tilt of $(\pi - \beta)$. This alteration leads to the change of signs of cosine functions which then makes the ground reflected irradiation contribution higher compared to the diffuse irradiation. By applying the first modification to Equation (14), we get:

$$I_{t,back} = I_b R_b + I_d \left(\frac{1 - \cos\beta}{2} \right) + I\rho_g \left(\frac{1 + \cos\beta}{2} \right) \quad (15)$$

Second modification: The Ratio of Beam Radiation, R_b

There are several articles on the modelling of the field performance of bifacial PV modules (Louw & Rix, 2019; Marion et al., 2018; Shoukry, Berrian, Libal, & Haffner, 2018; Shoukry et al., 2016; Wang et al., 2015a; Ufuk Alper Yusufoglu et al., 2014) . However, most of them ignores the beam radiation incident on the rear surface of bifacial PV modules. In this study, we include the beam irradiation contribution on the rear surface. To take beam irradiation into account, the period of hours when the Sun is directly on the rear side is determined. When the Sun is at low altitude, the angle of incidence of the solar irradiation is greater than 90° , i.e. the Sun is behind the surface (Duffie et al., 1985, p. 14). The angle of incidence is calculated according to the Equation (4). For these hours, the ratio of beam factor for the rear side $R_{b,back}$ has been determined. First, the ratio of beam R_b values for the front surface has been calculated according to Equation (11), and then for $R_{b,back}$ values, the

following $R_{b,front}$ values are taken. The reason is that the path of the Sun is symmetric concerning the passage of time. The representation of the Sun's path is given in the Figure 2.3.

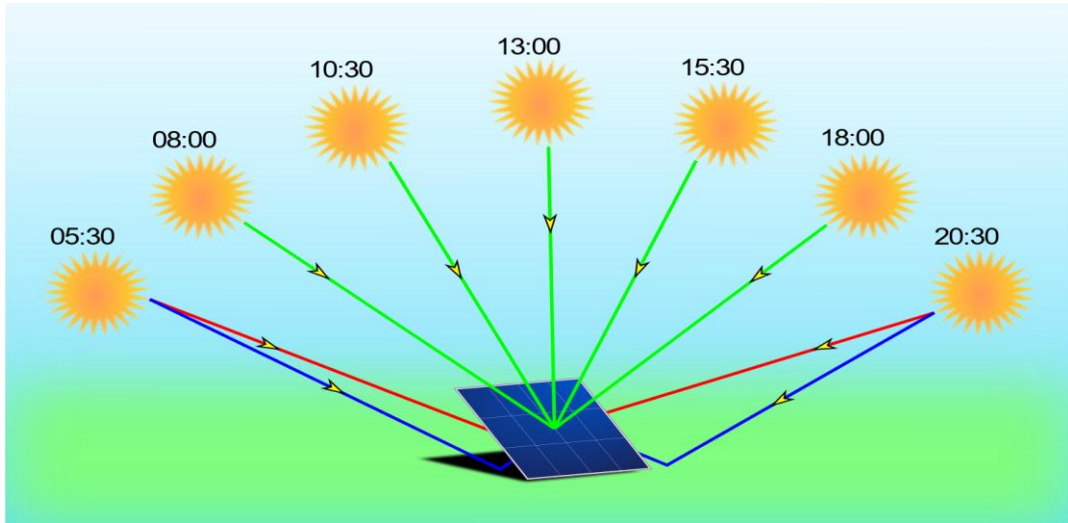


Figure 2.3. A representation of the Sun's path during summer. Here, green arrows indicate the radiation incident on the front surface between the hours 08:00 and 18:00, and red arrows imply that the Sun is behind the surface and there is beam contribution of the sunlight on the rear surface during the sunrise and the sunset. Blue arrows show the ground reflected radiation on the rear surface.

All mentioned calculations have been done for the hours between the sunrise and the sunset. For the hours when the ratio of beam R_b , front values are smaller than zero, it is assumed that there is no beam contribution for that period. An example set of the $R_{b,back}$ calculation for an arbitrary day, is given below in Table 2.1. The blue numbers are for the hours that the Sun shines to the rear side. The red numbers are the numbers we use for $R_{b,back}$, as shown in the last column using the symmetry consideration above.

Table 2.1 $R_{b,back}$ calculation between sunrise and sunset for an arbitrary day.

Hour	$R_{b,front}$	θ	$R_{b,back}$
05:00	0.00	113.34	0.66
06:00	0.00	100.31	0.21
07:00	0.21	86.892	0
08:00	0.66	73.3	0
09:00	0.83	59.694	0
10:00	0.92	46.276	0
11:00	0.97	33.454	0
12:00	0.99	22.434	0
13:00	1.00	17.251	0
14:00	0.99	22.434	0
15:00	0.97	33.454	0
16:00	0.92	46.276	0
17:00	0.83	59.694	0
18:00	0.66	73.3	0
19:00	0.21	86.892	0
20:00	6.66	100.31	0.21
21:00	3.96	113.34	0.66

In this study, all calculations are done for the hours between the sunrise and the sunset. Negative values of $R_{b,front}$ front have been taken as zero. With the second modification, Equation (15) can be written as:

$$I_{t,back} = I_b R_{b,back} + I_d \left(\frac{1 - \cos\beta}{2} \right) + I\rho_g \left(\frac{1 + \cos\beta}{2} \right) \quad (16)$$

Third modification: Elevation function

One of the parameters that affects the rear side irradiation is the elevation, i.e. the height of the module from the ground. Several articles analyze the effect of elevation on the efficiency of a bifacial PV module (Asgharzadeh, Lubenow, et al., 2018; Asgharzadeh, Marion, et al., 2018; Deline et al., 2017; Hansen et al., 2017; Valdivia et al., 2018; Wang et al., 2015b). According to the findings of the mentioned articles, the efficiency increases with increasing elevation up to a certain level. The reason is that modules with high elevation from the ground are less prone to the self-shading. Increasing the elevation of the module enhances the performance of the module up to a point at which the self-shading diminishes. This saturation height level is beneficial since it reduces installation costs (Sun, Khan, Deline, & Alam, 2018).

The elevation becomes significantly essential for bifacial solar modules since it is directly related to self-shading. Shadows cast on the ground lower the value of ground reflectance, meaning that the incoming solar irradiation is reflected from the shadow, not from the ground. Therefore, it is crucial to take elevation into account for the estimation of the rear side irradiation.

To observe the effect of elevation on the rear side irradiation, we have set up three configurations of two pyranometers at different elevations on the rear side of the bifacial PV module. Since different parts receive varying amounts of the ground reflected irradiation a correction factor might be used for the rear irradiation as follows:

$$I_{t,back} = I_b R_{b,back} + I_d \left(\frac{1-\cos\beta}{2} \right) + I \rho f(h) \left(\frac{1+\cos\beta}{2} \right) \quad (17)$$

To account the differences between these irradiation values, a distribution function of elevation can be used from which an average value for the correction factor can be deduced. This function should be integrated in the interval of 0.5 m to 1.16 m (min. and max. height of the module from the ground, respectively). The distribution function should be exponential as the rear surface irradiation from bottom to up does not increase uniformly:

$$F(l) = 1 - e^{-l/l_c} \quad (18)$$

Critical length constant l_c can be calculated by assuming that the value of the function at mid-length of 0.84 m to be 0.5:

$$0.5 = 1 - e^{-0.84/l_c} ; \quad (19)$$

which then gives:

$$l_c = 1.21.$$

To find an average value for this factor, one can use the following averaging integration:

$$\langle f(h) \rangle = \int_{0.5}^{1.16} (1 - e^{h/1.21}) dh \quad (20)$$

which gives:

$$\langle f(h) \rangle = 0.33$$

Here we assumed that the average correction factor is normalized out of the maximum possible correcting value of 1. Thus, for a bifacial solar module, we have found that average correction factor $\langle f(h) \rangle = 0.33$. Using this value in Equation (17), we reached the model calculation of solar irradiation impinging on the rear side as:

$$I_{t,back} = I_b R_{b,back} + I_d \left(\frac{1 - \cos\beta}{2} \right) + 0.33 I_{\rho_g} \left(\frac{1 + \cos\beta}{2} \right) \quad (21)$$

2.4 PV Yield Calculation

In order to make feasibility studies, it is crucial to estimate the yield of a PV module or an array. Many tools enable us to calculate the energy yield of a commercial

(monofacial) PV module. In this study, we have used the methodology of PVForm which is developed by (Menicucci & Fernandez, 1989). Since there is not a commercially available extension tool for the bifacial PV module, we have used the same methodology for the rear surface and treat the rear side the same with the front.

PVForm calculates the plane-of-array irradiance according to modified version of Perez 1990 algorithm (Perez, Ineichen, Seals, Michalsky, & Stewart, 1990), and treats the diffuse radiation as isotropic for the zenith angles between 87.5 and 90 degrees (NREL & Dobos, 2014).

$$I_{poa} = I_b + I_{d,sky} + I_{d,ground} \quad (22)$$

However, there is an angle of incidence (AOI) correction that applies to incidence angles higher than 50 degrees. The reason is to find the transmitted irradiance by considering reflection losses, and it is calculated as follows (NREL & Dobos, 2014):

$$f = b_0 + b_1\theta + b_2\theta^2 + b_3\theta^3 + b_4\theta^4 + b_5\theta^5 \quad (23)$$

$$I_{tr} = I_{poa} - (1 - f) I_b \cos(\theta) \quad (24)$$

where $b_0, b_1, b_2, b_3, b_4, b_5$ are module cover polynomial coefficients and equal to 1.0, -2.438E-3, 3.103E-4, 1.246E-5, 2.112E-7, -1.359E-9 accordingly. I_{tr} is the transmitted irradiance, I_b is the beam component, and θ is the angle of incidence.

To find the module temperature, a thermal model developed by (King, Boyson, & Kratochvill, 2004, pp. 18–20) is integrated into the PVForm methodology. To calculate the operating module temperature, the total irradiance, wind speed, ambient temperature, and empirical constants have been used according to the model.

The model calculates the DC power output by adjusting the array efficiency for the irradiation values that are less than 125 W/m².

$$P_{dc} = \frac{I_{tr}}{1000} P_{dc0} \left(1 + \gamma(T_{cell} - T_{ref}) \right) \quad I_{tr} > 125 \text{ W/m}^2 \quad (25)$$

$$P_{dc} = \frac{0.008 I_{tr}^2}{1000} P_{dc0} \left(1 + \gamma (T_{cell} - T_{ref}) \right) \quad I_{tr} \leq 125 \text{ W/m}^2 \quad (26)$$

The temperature coefficient $\gamma = -0.5\%$, $T_{ref} = 25 \text{ }^\circ\text{C}$ and P_{dc0} is the nameplate DC rating.

There are a few modifications that we have done for the estimation of bifacial PV yield. First, the declination and the angle of incidence values are calculated by using more accurate Equations (2) and (4), respectively. Secondly, we have calculated I_{poa} for the front and the rear surface (namely, I_t and $I_{t,back}$ in our context) by using Equations (14) and (17), and then, I_{tr} and $I_{tr,back}$ is calculated. For $I_{tr,back}$ calculation, instead of filtering data for the incident angles, we have applied the AOI correction for the hours when there is a beam irradiation incident on the rear surface, meaning that $R_{b,back}$ is greater than zero. After finding the DC power output for both surfaces, we have add them up to find the total DC power output.

The methodology of the estimation of the bifacial yield is represented as a flow chart in the following section.

2.5 Bifacial Yield Modelling

Modeling is a mathematical or conceptual way of representing a real system. Models enable us to predict the performance that can be measured. In the scope of PV modeling, the performance analysis of a PV module under a wide range of location and installation dependent parameters can be done. The effect of such parameters on the efficiency of a PV module is analyzed, and then, the optimal conditions for installation can be determined. For a monofacial PV module, many simulation tools like MATLAB PVLlib, Helioscope PVSYS, SAM, and INSEL have been developed to interpret the performance of the module in terms of defined parameters. However, for a bifacial PV, there is no defined set of parameters to analyze the performance of the bifacial PV module by using mentioned or any other kind of simulation software program. The presented model includes our methodology for

estimating the rear side irradiation and a modified version of PVForm methodology. Overall, the model uses a few inputs related to the location and the system properties. Table 2.2. shows the required parameters for the bifacial yield calculation part of the model.

Table 2.2 The set of system parameters that are required for PVWatts calculator is listed below for our configuration.

Field	Units	Value
System Size	kW (DC)	0.295
System Derate	fraction	Not Applicable
Array Tracking Mode	Fixed, 1-axis, 2-axis	Fixed
Tilt Angle	degrees	32
Azimuth Angle	degrees	0

Solar irradiation reaching to Earth through the atmosphere converted to the electrical energy by reaching to a PV module. Through this conversion, some portion of the energy is transferred, and some portion of it is lost. It is crucial to include losses in this process, and PV performance models enable us to calculate how much of the energy is useful for electricity. However, including each modelling step becomes beyond this research in terms of time and resources. Instead, the focus is on the optical behavior of a PV module and estimating the incident irradiation on the plane of the module. Figure 2.4. shows the sequence of a single bifacial PV model performance modelling steps.,

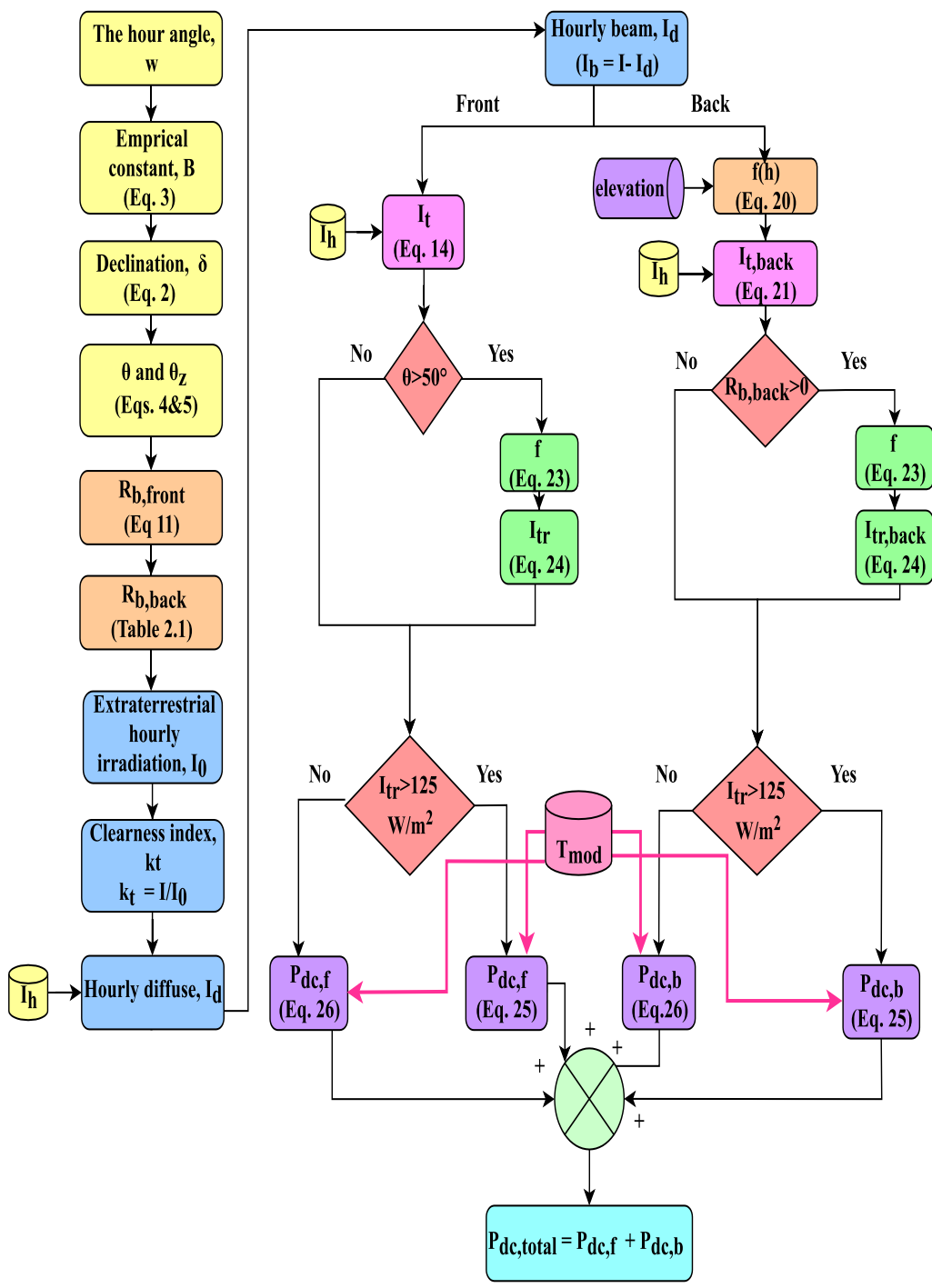


Figure 2.4. A sequence of a bifacial PV yield modelling

CHAPTER 3

OUTDOOR TESTING SITE AND MEASUREMENTS

3.1 Test Site and the Module

The test site is on the rooftop of the Physics department at METU, Ankara (Central Anatolia). The climate of the test site is hot and semi-arid warm temperate (Peel, Finlayson, & McMahon, 2007). The yearly total precipitation for last 30 years is 388.1 mm. The average monthly temperature is about 12 °C. For July and August, the maximum temperature rises to 30°C and for January, the minimum temperature drops to -3°C (State Meteorological Service of Turkey; <https://www.mgm.gov.tr>) The geographical information of the test location is given in Table 3.1.

Table 3.1 Summary of the geographical information of the test location.

Parameter	GUNAM-Ankara, Turkey
Latitude	39.9°N
Longitude	32.8°E
Elevation	920 m
Azimuth angle (S=0, E=-90)	0 °

There are 16 test beds for monitoring the performance of PV modules in the test platform. These test beds are convenient for different types and frame structure of PV modules. The facility at the rooftop of the Physics Department in METU campus and the representation of all components in the test facility are below in Figure 3.1 (a) and (b). The test platform has a 32° tilt angle and all PV modules are at the same tilt.

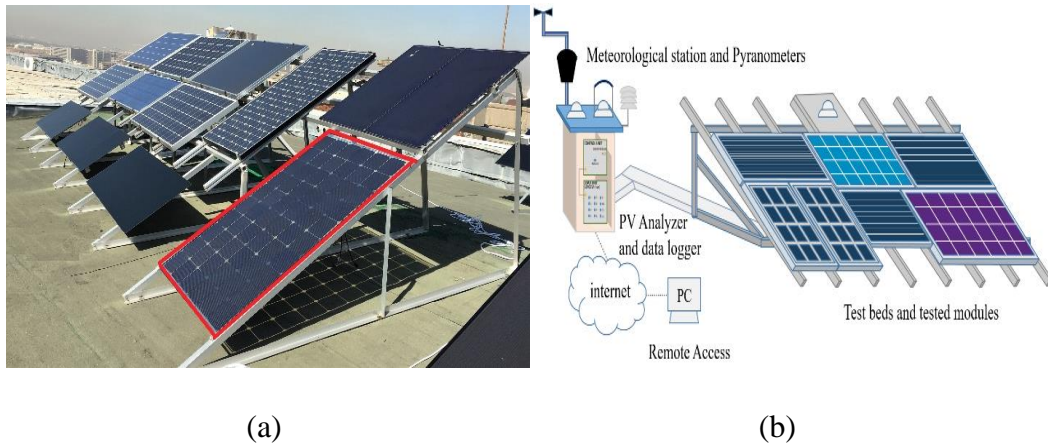


Figure 3.1. (a) Outdoor Test Facility in GUNAM, METU. The tested bifacial module is indicated by the red rectangle. (b) Representation of all components in the test facility.

3.2 Measurement System

In GUNAM Outdoor Test Facility, a measurement device, Daystar Multi Tracer 5, is used as it is used in the National Renewable Energy Lab as well. Daystar Multi Tracer 5 has two parts: the control and the load unit. The control unit measures the module temperature. Figure 3.2 shows the test and the cabin of Daystar Multi Tracer 5.



Figure 2.2 Test site and the cabin of multi tracer

The load unit has 16 available channels that connect testbeds to the terminals of PV modules. During the daytime, when the modules are working actively, the produced current passes through the load, and terminal voltage and current values of modules are measured at pre-specified instants. Daystar Multi Tracer 5 is a network device, i.e., it connects to a computer network via ethernet cables. Therefore, the data contained in the storage is easily accessible from any location. Besides, the device also takes periodic I-V curves for each module (<http://www.daystarpv.com/multitracer3.html>) Performance parameters can be measured as average, instantaneous, or both. The performance parameters are given in the Table 3.2.

Table 3.2. Summary of the parameters that the test device measures for the performance assessment of PV modules

Measurement type	Parameters
Instantaneous	V_{oc} (V), V_{max} (V), I_{sc} (A), I_{max} (A), P_{max} (W), FF (%), $T_{ambient}$ ($^{\circ}C$), T_{module} ($^{\circ}C$), $Irradiance_{horizontal}$ (W/m^2), $Irradiance_{tilted}$ (W/m^2)
Average	V_{max} (V), I_{max} (A), P_{max} (W), $T_{ambient}$ ($^{\circ}C$), T_{module} ($^{\circ}C$) $Irradiance_{horizontal}$ (W/m^2), $Irradiance_{tilted}$ (W/m^2)

3.2.1 Environmental Measurements

All meteorological data have been recorded since 2015. The weather stations can measure: rainfall (mm), pressure(millibar), ambient temperature ($^{\circ}C$), relative humidity (%), horizontal total solar radiation(W/m^2), UV (MEDs), wind speed(m/s) and direction ($^{\circ}$). In addition to meteorological measurements, there are also two black and white high precision pyranometers to measure both horizontal and tilted irradiance. Both the weather station and pyranometers record measurements in each 10 minutes. The meteorological station's data can be easily downloaded by using a

web portal with remote access through its desktop software. Figure 3.3 shows the weather station and pyranometers.



Figure 3.3. Meteorological Station (Davis Vantage Pro2+) and sensors (Kipp&Zonen CMP11)

3.2.2 PV Module and Measurement Configurations

The yield measurements of the modules have been carried out since 2012. The collected data of Multi Tracer can be easily accessed by using ftp protocol.

In this study, we have used a single bifacial PV module. The characteristics of the module are given in Table 3.3. The module is mounted on one of test beds mentioned before. Its front side is 0.5 m above from the ground. The ground type is a gray shingling with 0.2 ground reflectance (albedo).

Table 3.3. Summary of the properties of the bifacial PV module

Module Types	P_{NOM} [W]	P_{MAX} [W]	V_{OC} [V]	I_{SC} [A]	V_{MPP} [V]	I_{MPP} [A]	Tilt _{angle} [°]	Area [m ²]
Bifacial	290.0	294.6	44.10	8.8	35.7	8.3	32	1.61

Three different setups have been constructed to observe the effect of elevation on the performance of the bifacial PV module. Two pyranometers have been placed at the

rear side of the bifacial PV module at three different height levels, two levels at a time. Figure 3.4 shows three configurations of the pyranometers on the rear side of the bifacial PV module. The data is taken for three days for each configuration. The first configuration involves one pyranometer at the middle and the other at the bottom, 0.84 m and 0.50 m above the ground, respectively. For the second configuration, we have placed the pyranometer at the bottom to the top (0.50 and 1.16m above the ground). As a final step, for the third configuration, we removed the one in the middle and placed it to the bottom (1.16 and 0.50 m above the ground).

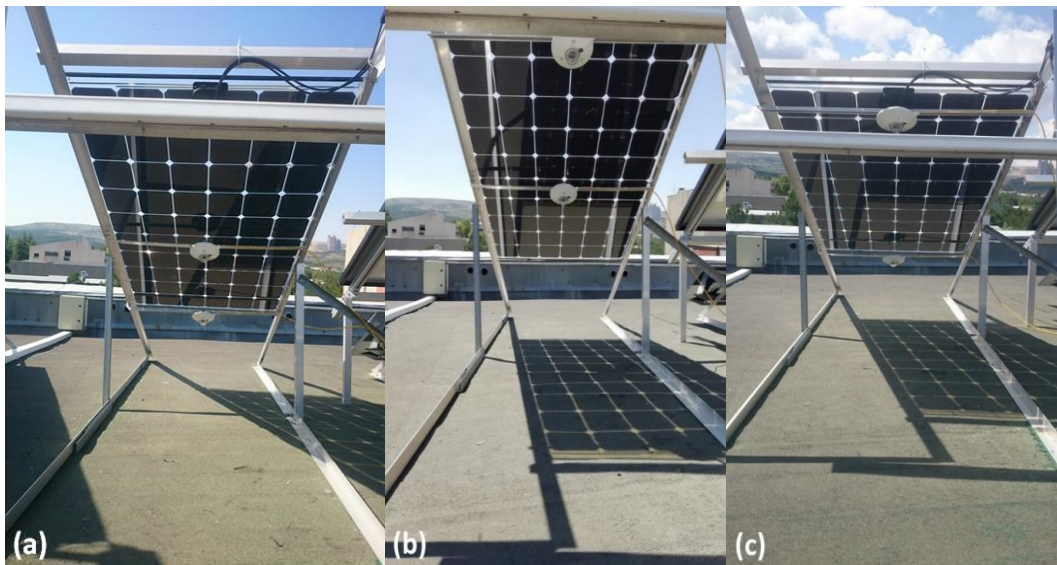


Figure 4.4 (a) First configuration with one pyranometer is at the bottom-back (0.50 m) and the other is at the middle-back (0.84m). b) Second configuration with one pyranometer is at the top-back (1.16 m) and the other is at the middle-back (0.84 m) c) Third configuration with one pyranometer is at the bottom-back (0.50 m) and the other is at the top-back (1.16 m)

3.3 Verification Methods

It is critical to test the accuracy of the model by using statistical approaches and then reliability of the model can be assured. Mean bias error (MBE), mean absolute error (MAE), and the root mean square error (RMSE) analysis methods are widely used statistical models.

The MBE and RMSE are two of most common approaches when it comes to find the accuracy. While many studies present RMSE as the standard metric for accuracy testing (Chai & Draxler, 2014; Chai et al., 2013; Savage et al., 2012), some prefers only MAE which measures the average magnitude of the errors in a positive set. (Chatterjee, Engelen, Kawa, Sweeney, & Michalak, 2013; Jerez et al., 2013; Taylor, Losch, Wenzel, & Schröter, 2013; Willmott, Matsuura, & Robeson, 2009). Therefore, MAE method also applied in the verification. Three test methods can be found according to following formulas

$$MBE = \frac{1}{n} \sum_i^n c_i - m_i \quad (27)$$

$$MAE = \frac{1}{n} \sum_i^n |c_i - m_i| \quad (28)$$

$$RMSE = \sqrt{\frac{1}{n} \sum_i^n (c_i - m_i)^2} \quad (29)$$

The ideal value of MBE, MAE and RMSE is zero, and MAE and RMSE gives always positive value or zero.

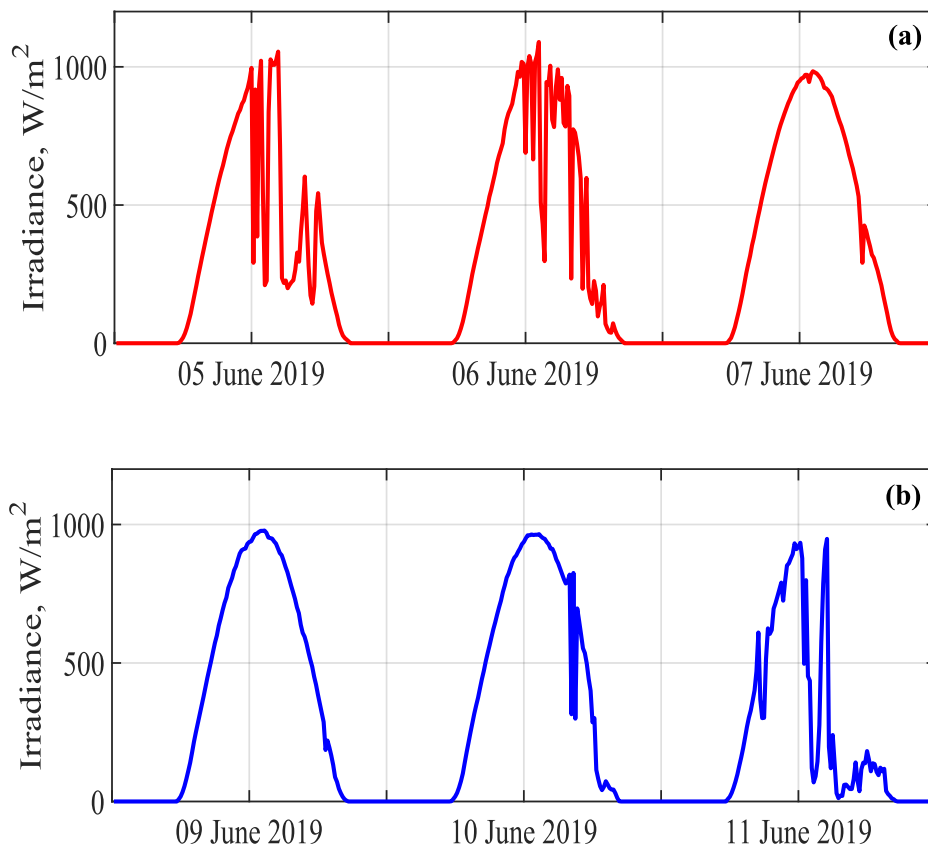
The model is verified using three statistical methods mentioned above, and the results will be given in the Table 4.1.

CHAPTER 4

RESULTS AND DISCUSSION

4.1 Solar Irradiation

As mentioned before in previous sections, it is critical to estimate the rear side irradiation. In this presented model, we have managed to calculate the rear side irradiance. Measurements have been carried for both clear and cloudy days to see how the model behaves for cloudy days. During the measurement procedure, the horizontal irradiance had been measured by the Davis instrument. The days that we carried out these measurements are presented in Figure 4.1; (a), (b), and (c) correspond to configurations (a), (b), and (c) of Figure 3.4, respectively.



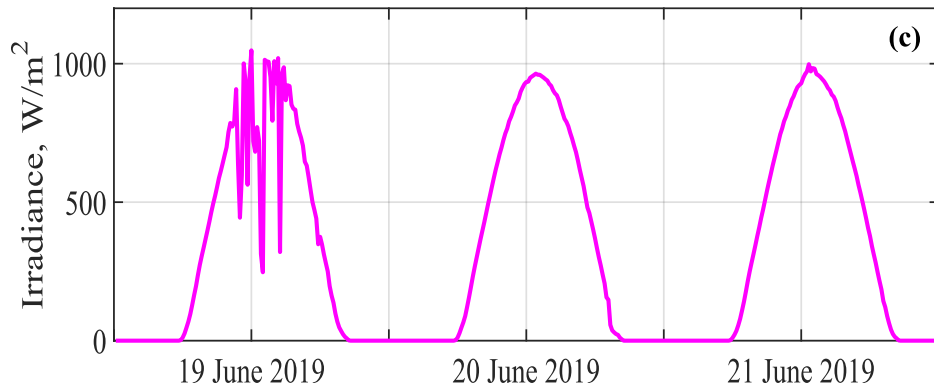
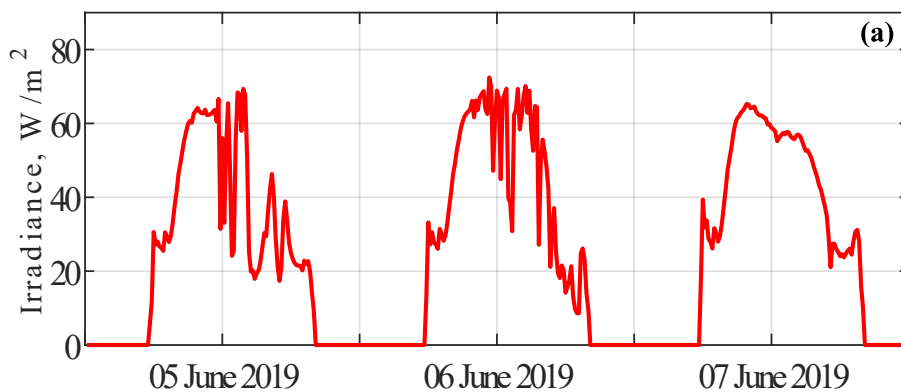


Figure 4.1. Horizontal irradiance measurements simultaneously with rear side irradiance measurements for (a) first configuration (b) second configuration (c) third configuration

Figure 4.2–(a), (b), (c) shows the rear side irradiance measurements for the above three typical days for three configurations. The solar irradiance on the rear side is much lower than that of on the horizontal surface. One of the reasons is that the front surface receives more of the beam radiation than the rear side. Another reason is that the device that measures the horizontal irradiance is always prone to sun rays between the sunrise and the sunset. Besides, it is not affected by the shading, unlike the pyranometers on the rear side of the bifacial PV module. Results also show that the tested bifacial module does not have optimal mounting conditions, and the ground reflectance is remarkably small, therefore with the shading, it gets even much smaller.



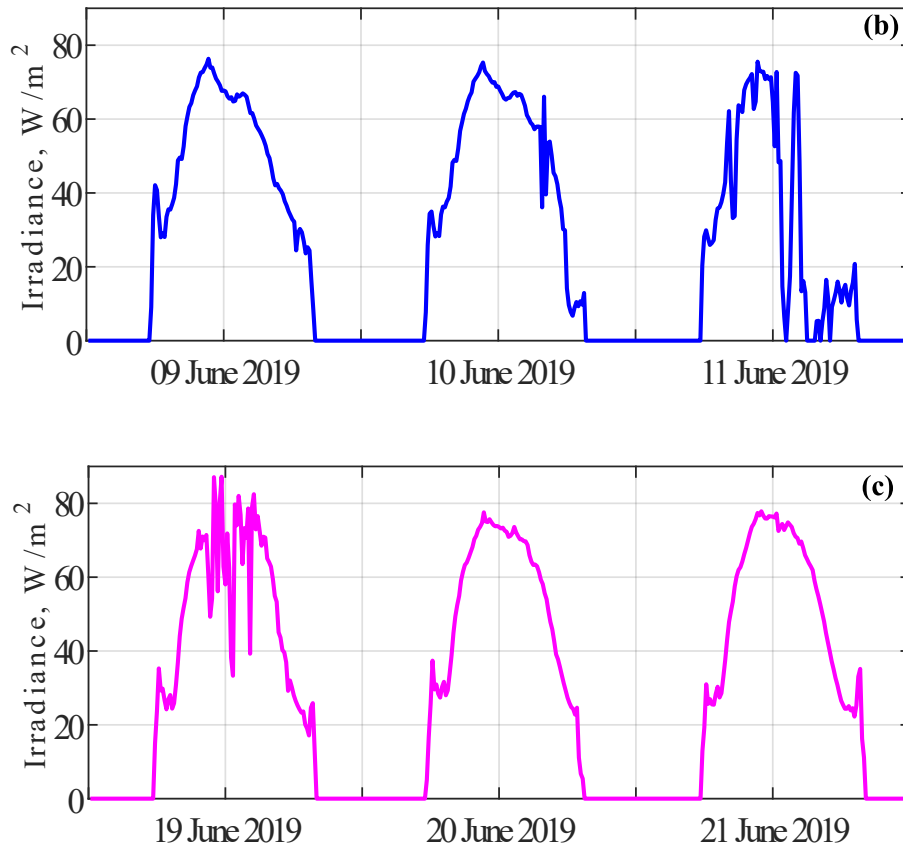


Figure 4.2 Rear side irradiance measurements for (a) first configuration (b) second configuration (c) third configuration

As can be seen in Figure 4.2 (a), (b), (c) the portions of solar irradiation reaching the surface are different for each configuration. As mentioned before, there are several studies (Asgharzadeh, Lubenow, et al., 2018; Asgharzadeh, Marion, et al., 2018; Deline et al., 2017; Hansen et al., 2017; Valdivia et al., 2018; Wang et al., 2015b) on the effect of elevation of the module on the performance of bifacial modules. According to these studies, the efficiency of a bifacial module increases as the elevation increases up to 1 meter. In consideration of this, we expected that we would have higher solar irradiance for the second configuration with one pyranometer on the top, and the other is in the middle. To make a fair comparison, we have chosen one clear and one partially cloudy day in which the rear side irradiances are compatible and then sketched the irradiances for bottom, middle and top part of the rear side. Estimations are done for both clear and cloudy days. The average radiation

incident on the rear surface for both days is almost the same since beam contribution is not significant, unlike monofacial modules. Figure 4.3 (a), (b) shows the rear side irradiances compiled like a one whole day for three levels of height. As can be seen from that figure, the top-back side of the module receives the most of solar irradiation. Although we have expected that the bottom-back would receive the least amount of solar irradiation, at noon hours, it happens to be the middle-back part.

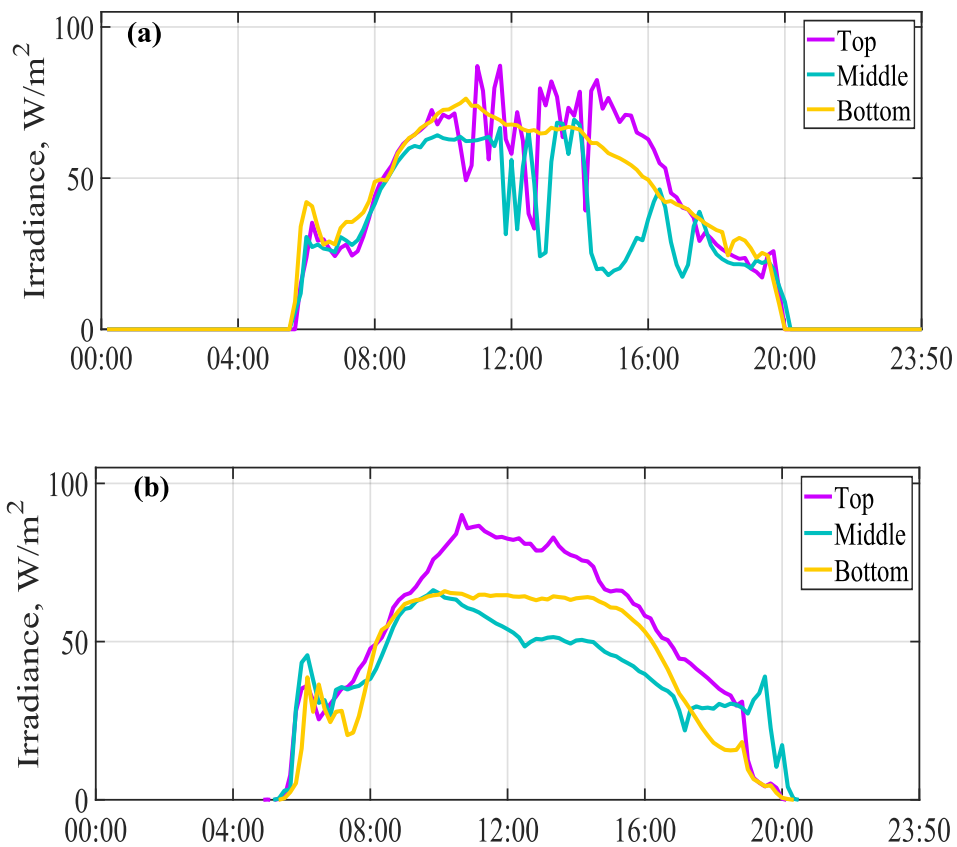


Figure 4.3. Rear side irradiances compiled like a one day for three elevations (a) For a cloudy day, 19 June 2019 (b) For a clear day, 20 June 2019

To find out the reasoning behind why the middle part receives more sunlight than the bottom part, on a clear day during a site visit, we have seen that most of the time, nearby modules and the bifacial module itself cast shadows on the middle part of the module. That means the radiation is reflected from the shadow, which reduces the reflectance of the ground.

As a result, the third component of the Equation (17) gets smaller for the second configuration. Figure 4.4 shows the shading path on a partially cloudy day.



Figure 4.4. The shading path on a partially cloudy day.

The analysis of the difference between the irradiance incident on the bottom, middle and the top region of the rear side might be useful, yet this is our further research of interest. Thus, in this work we used average correction factor $\langle f(h) \rangle = 0.33$ as stated in chapter 2. The solar irradiation incident on the rear side of the bifacial PV module is calculated by using Equation (17) which is a modified version of the Liu and Jordan's isotropic sky model. Figure 4.5-(a), (b) and (c) give the measured average values of the rear side irradiation and the estimated values using the modeling approach described above for three days.

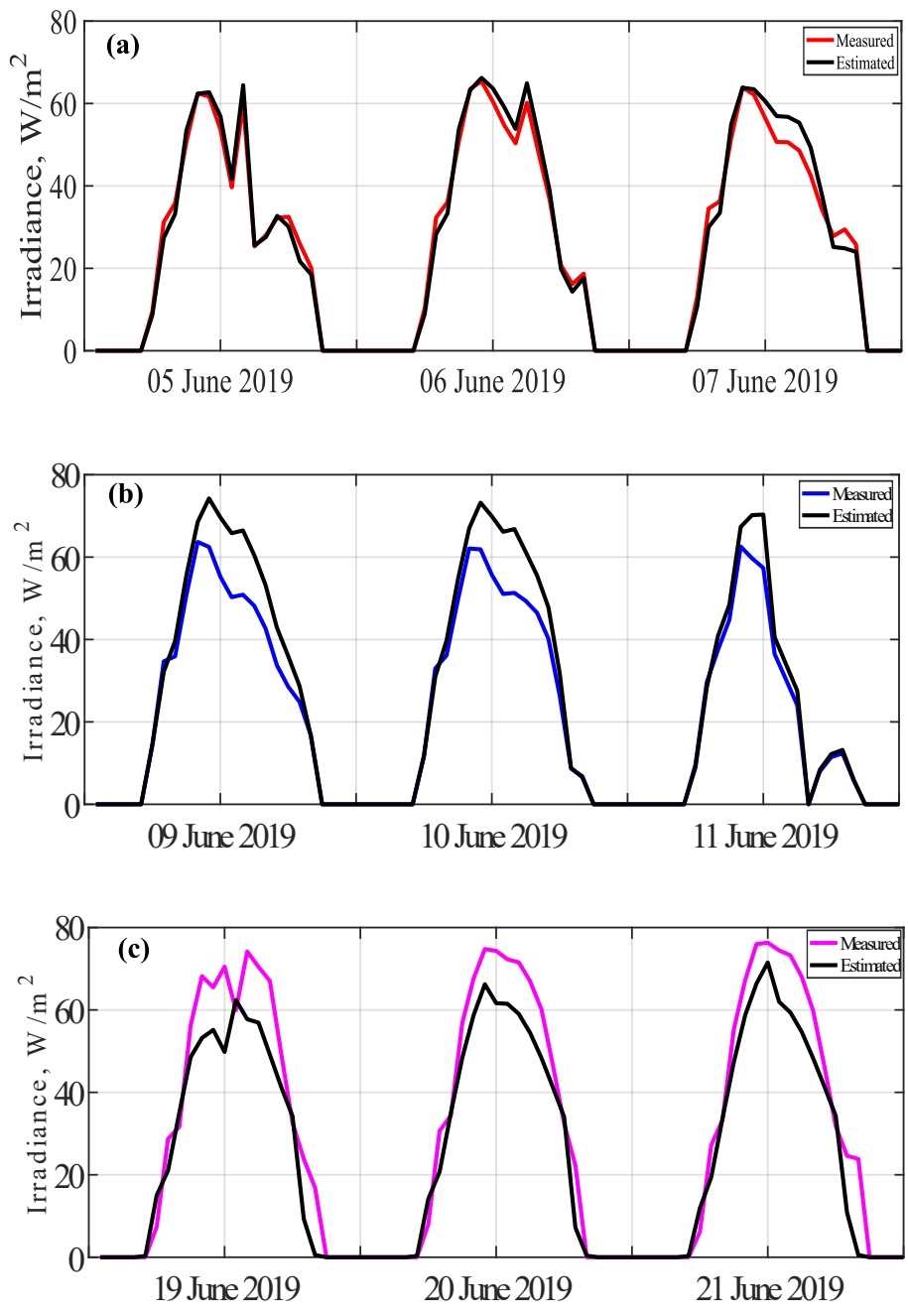


Figure 4.5. Measured and estimated rear side irradiances for (a) first configuration (b) second configuration (c) third configuration

The results showed that estimated and measured rear side solar irradiation values agree quite well, as shown in Figure 4.5. As can be observed in Figure 4.5-(c), when the pyranometers are placed at the middle and bottom rear side, the model slightly

underestimates, while for the other two configurations, the estimations are much better. One of the reasons of the underestimation is the shading of the module itself and nearby modules concentrated on the middle part. Therefore, the pyranometer measures the irradiance that is reflected from the shadow, not from the ground. The model does not consider the shading by the typical urban type ground. However, the overestimation is within acceptable levels, and results are verified using some statistical approaches in the following Table 4.1. For all configurations, it is seen that there are slight shifts between the measurements and estimations. This is mainly because of the accuracy of the Davis instrument (which measures the horizontal irradiance) and pyranometers (that measure the rear side irradiance). The Davis instrument cannot merely catch the horizontal irradiance within the precision of the pyranometer. That leads to shifts in the rear side irradiation estimations since the rear side irradiation is calculated by using the horizontal irradiation.

Table 4.1. Results of statistical error calculations by using three different methods for each configuration

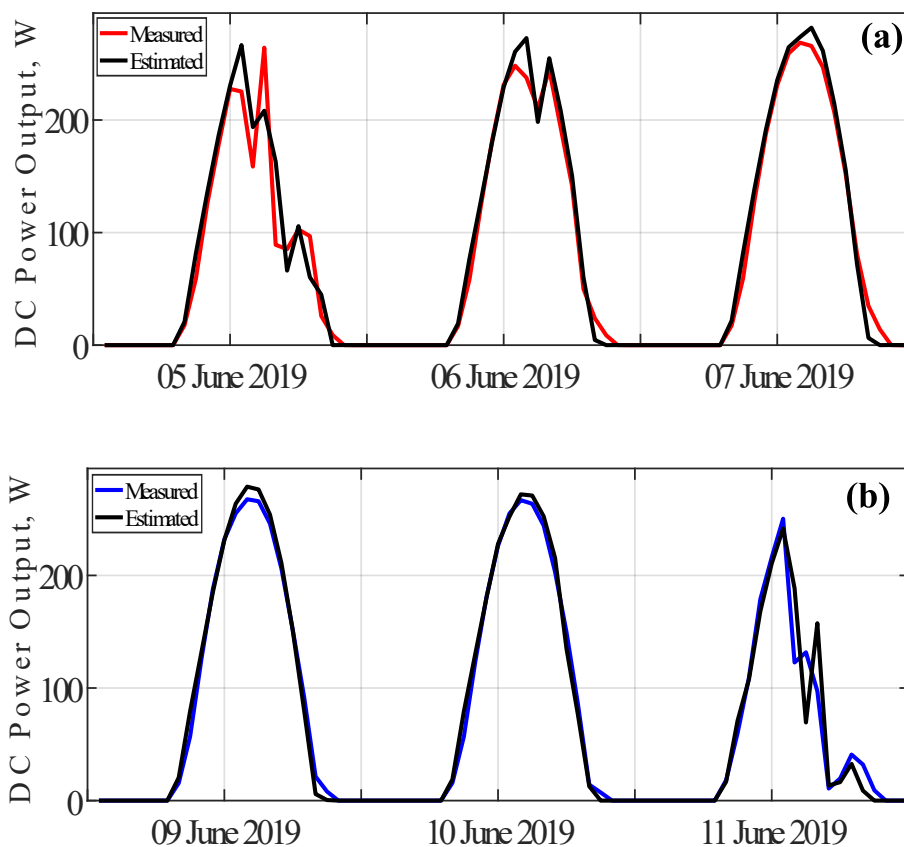
Day	MBE(W/m ²)	MAE(W/m ²)	RMSE (W/m ²)
5 Cloudy	-0.08	1.26	1.95
6 Cloudy	0.56	1.58	2.28
7 Clear	0.81	1.58	2.28
9 Clear	4.63	4.85	7.39
10 Cloudy	4.23	4.42	6.99
11 Cloudy	4.23	4.42	6.99
19 Cloudy	-5.53	6.81	9.73
20 Clear	-4.48	5.24	7.50
21 Clear	-4.48	5.24	7.50

The results showed that estimated and measured rear side solar irradiance values agree quite well. From statistical error calculations of the rear side irradiation estimations, the minimum and maximum values of MBE are -0.08 W/m² and -5.53 W/ m², respectively. The minimum and maximum RMSE values for the same estimation are 1.95 W/m² and 9.73 W/m². There is a slight underestimation for the third configuration. The reason is that the lower and upper parts of the module

receive more illumination than the middle section. However, the underestimation is within acceptable levels, yet the shading effect to the ground reflection is another research outcome of the present work about bifacial modules and arrays.

4.2 Bifacial PV Yield

To estimate the bifacial PV yield, we have used a modified version of PVWatts methodology. The estimated yield and the measured yield agree quite well. While the maximum estimated yield is 282 Watt, the measured yield (including cable losses and degradation) is 268.68 Watt for the same day. Figure 4.6 shows the estimated and measured bifacial PV yield for three configurations.



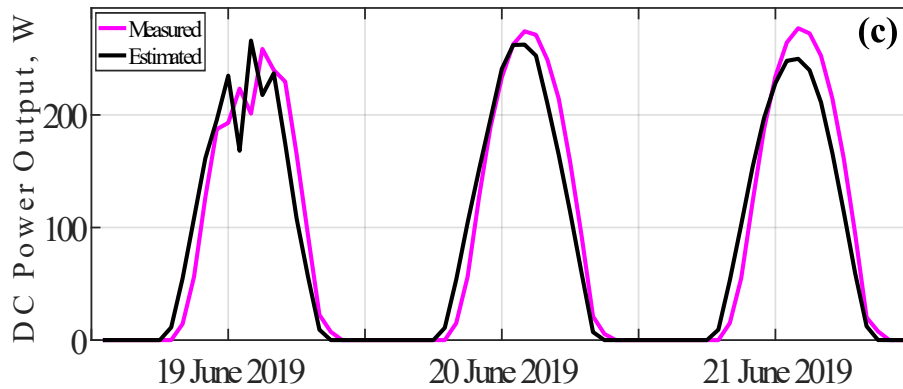


Figure 4.6. Measured and estimated DC power output for (a) first configuration (b) second configuration (c) third configuration

From Figure 4.6, it is seen that the model slightly overestimates the DC power output for the first and the second configuration, and there is underestimation for the third configuration. To make a better comparison of the estimated and measured values, the statistical error approach has been used, and the results of daily statistical error calculations for bifacial PV yield are given in Table 4.2.

Table 4.2. Results of statistical error calculations for bifacial PV yield by using three different methods for each configuration for two different days.

Day	MBE(Wh)	MAE(Wh)	RMSE (Wh)
5 Cloudy	4.11	14.15	24.46
6 Cloudy	3.06	6.70	10.92
7 Clear	1.94	6.23	9.91
9 Clear	1.56	4.80	7.64
10 Cloudy	1.27	4.30	7.13
11 Cloudy	0.26	11.40	23.19
19 Cloudy	-0.62	21.74	31.82
20 Clear	-3.33	14.72	22.73
21 Clear	-5.59	16.90	24.66

From Table 4.2., estimated and measured values agree better for clear days, and there is a bit more deviation for cloudy days. Besides, the maximum RMSE difference occurs for a cloudy day for the third configuration. The reason might be the accuracy

of the rear side irradiation calculation. To improve the results, instead of the isotropic sky approach, anisotropic sky model can be implemented on the rear side irradiation calculation. Besides, a better value of $f(h)$ can be obtained by comparing the theoretical calculation using long term such measurements at different climatic conditions. To make the verification of the model more comprehensive, monthly energy yield for a year is calculated. Figure 4.7 shows the monthly bifacial yield over a year.

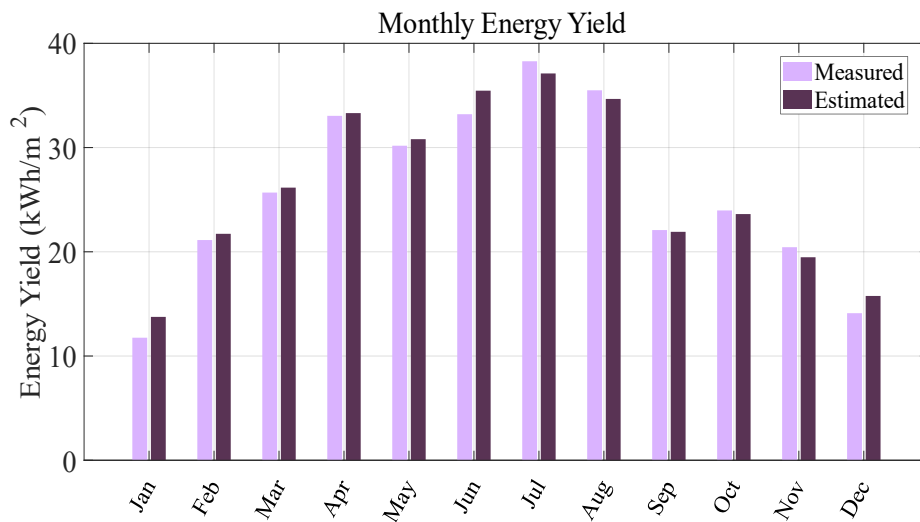


Figure 4.7. Monthly estimated and measured energy yield of a bifacial PV yield over a year.

From Figure 4.7, monthly energy yield calculations are much more better than daily estimates. There is an overestimation only for January but this is because of the heavy snowfall during that month. For annual bifacial PV yield estimations, the model has a relative percent error approximately equal to 1.4%. The presented model can be inserted to the efficiency calculations of bifacial PV modules/arrays or can be used for long term simulation purposes.

CHAPTER 5

CONCLUSION

In this study, the theory of bifacial PV module technology was briefly discussed, and a model to estimate the rear side irradiation incident on the bifacial PV module is described. The yield of the module is also modelled, calculated and compared with the measurements. Both measurements and statistical analysis methods verified the proposed model.

Based on the gained theoretical literature, monofacial and bifacial modeling approaches are compared. Two conventional approaches, view factor and ray-tracing methods for bifacial PV modeling, have been discussed in terms of their advantages and disadvantages. The presented model in this thesis is based on Liu & Jordan's isotropic sky model. Three modifications were applied to that model. The first modification is altering the tilt angle for the rear surface. Secondly, the ratio of the beam radiation factor for the rear side is estimated. Lastly, a function of elevation factor is used for the ground reflected radiation component.

All calculations are done by using Microsoft Excel & MATLAB for hours between sunrise and sunset. The energy yield of the bifacial PV module is done by using PVForm methodology. The proposed model for the rear side irradiance is integrated into the PVForm. To evaluate the performance of the bifacial PV module, MBE, MAE, and RMSE analysis practiced in this study. Although there were arguments about these statistical analyses being useful indicators, and there were some inconsistencies between three test methods, all methods result in acceptable error margins.

At some point, the world will face an energy crisis due to the growing population. One way to meet the energy demand is by using renewable energy resources, mainly solar energy, since the Sun is the most sustainable resource we have. The developments in solar photovoltaic technology will increase the efficiency. Within

the acknowledgment of these developments, bifacial PV technology may replace the monofacial PV modules soon. To keeping up with changing technologies, feasibility studies of bifacial PV modules should be done by using simulation software programs or modeling approaches. Unfortunately, there is no commercially available tool yet. For this reason, in this study, a model for the estimation of the rear side irradiation incident on the rear surface and the bifacial PV yield is proposed.

In conclusion, the model presented here has significant contributions to the literature that were not addressed yet. The model does not require high computational power, unlike many models presented for the same purpose. Moreover, it can be easily adapted for any site or installation condition.

5.1 Future improvements

The proposed model will be improved for the bifacial yield calculations. Together with the rear side irradiation and the bifacial yield estimation, a complete algorithm can be composed, and then that algorithm can be included in SOIAR TURnKEY (Karaveli, 2018) which enables decision-makers to choose the most efficient PV technology for specific site/installation conditions. Therefore, the methodology proposed here would be beneficial for the feasibility analysis of bifacial PV technology.

In this study, measurements are carried out for a short period due to the lack of time and equipment. The next step is to take long term data for one year, at least. Besides, different configurations for installation can be set up to analyze the effect of albedo, the tilt angle, or shading.

Another way to improve the model is by repeating the same measurements for more than one bifacial PV module. In this way, we can observe how the model behaves for a bifacial PV array instead of a single bifacial PV module. For PV array case, shading can be an essential factor, and henceforth, shading effect would be included in the model as well.

To estimate the model performance on a longer-term, degradation analysis would be done. That analysis could be included in the model, along with other performance parameters. The model can be soft programmed, or a simulation tool can be constructed. With a user-friendly dialog box, module characteristics, installation, and location parameters would be given as inputs; then, the bifacial yield can be simulated.

REFERENCES

- Asgharzadeh, A., Lubenow, T., Sink, J., Marion, B., Deline, C., Hansen, C., ... Toor, F. (2018). *Analysis of the Impact of Installation Parameters and System Size on Bifacial Gain and Energy Yield of PV Systems*. <https://doi.org/10.1109/pvsc.2017.8366690>
- Asgharzadeh, A., Marion, B., Deline, C., Hansen, C., Stein, J. S., & Toor, F. (2018). A sensitivity study of the impact of installation parameters and system configuration on the performance of bifacial PV arrays. *IEEE Journal of Photovoltaics*, 8(3), 798–805. <https://doi.org/10.1109/JPHOTOV.2018.2819676>
- Bhattacharya, S., & John, S. (2019). Beyond 30% Conversion Efficiency in Silicon Solar Cells: A Numerical Demonstration. *Scientific Reports*. <https://doi.org/10.1038/s41598-019-48981-w>
- Bifacial Photovoltaics: Technology, applications and economics. (2018). In *Bifacial Photovoltaics: Technology, applications and economics*. <https://doi.org/10.1049/pbpo107e>
- Chai, T., & Draxler, R. R. (2014). Root mean square error (RMSE) or mean absolute error (MAE)?– Arguments against avoiding RMSE in the literature. *Geoscientific Model Development*, 7, 1247–1250. <https://doi.org/10.5194/gmd-7-1247-2014>
- Chai, T., Kim, H., Lee, P., Tong, D., Pan, L., Tang, Y., ... Stajner, I. (2013). Evaluation of the United States National Air Quality Forecast Capability experimental real-time predictions in 2010 using Air Quality System ozone and NO₂ measurements. *Geoscientific Model Development*, 6, 1831–1850. <https://doi.org/10.5194/gmd-6-1831-2013>
- Chatterjee, A., Engelen, R., Kawa, S., Sweeney, C., & Michalak, A. (2013).

- Chatterjee, A., R. J. Engelen, S. R. Kawa, C. Sweeney and A. M. Michalak (2013), Background error covariance estimation for atmospheric CO2 data assimilation, *Journal of Geophysical Research-Atmospheres*, 118 (17), 10140–10154, doi:10.1002/jgrd.50654. *Journal of Geophysical Research*, 118, 10140–10154.
- Cooper, P. I. (1969). The absorption of radiation in solar stills. *Solar Energy*, 12(3), 333–346. [https://doi.org/10.1016/0038-092X\(69\)90047-4](https://doi.org/10.1016/0038-092X(69)90047-4)
- Cuevas, A., Lague, A., & Ruiz, J. M. (1980). N** plus PN** plus DOUBLE-SIDED SOLAR CELL FOR OPTIMAL STATIC CONCENTRATION. *Conference Record of the IEEE Photovoltaic Specialists Conference*.
- Cuevas, A., Luque, A., Eguren, J., & del Alamo, J. (1982). 50 Per cent more output power from an albedo-collecting flat panel using bifacial solar cells. *Solar Energy*. [https://doi.org/10.1016/0038-092X\(82\)90078-0](https://doi.org/10.1016/0038-092X(82)90078-0)
- D.Faiman, & A.Dolev. (2004). Optimum orientation of bi-facial PV modules. *19th Eur. Photovoltaics Sol. Energy Conference*, 2470–2473. Paris, France.
- Deline, C., Macalpine, S., Marion, B., Toor, F., Asgharzadeh, A., & Stein, J. S. (2017). Assessment of Bifacial Photovoltaic Module Power Rating Methodologies-Inside and Out. *IEEE Journal of Photovoltaics*, 7(2), 575–580. <https://doi.org/10.1109/JPHOTOV.2017.2650565>
- Duffie, J. A., Beckman, W. A., & McGowan, J. (1985). Solar Engineering of Thermal Processes. In *American Journal of Physics* (Vol. 53). <https://doi.org/10.1119/1.14178>
- Fiore, J. M. (2018). Semiconductor Devices. *Proceedings of the IRE*, 50(5), 1006–1010. <https://doi.org/10.1109/JRPROC.1962.288388>
- Freris, L., & Infield, D. (2009). Renewable energy in power systems. In *Choice Reviews Online* (Vol. 46). <https://doi.org/10.5860/choice.46-4469>
- Goswami, D. Y. (2015). Principles of Solar Engineering. In *Journal of Solar Energy*

Engineering. <https://doi.org/10.1115/1.1288930>

- Guo, S., Walsh, T. M., & Peters, M. (2013). Vertically mounted bifacial photovoltaic modules: A global analysis. *Energy*. <https://doi.org/10.1016/j.energy.2013.08.040>
- Hansen, C. W., Stein, J. S., Deline, C., Macalpine, S., Marion, B., Asgharzadeh, A., & Toor, F. (2017). Analysis of irradiance models for bifacial PV modules. *2017 IEEE 44th Photovoltaic Specialist Conference, PVSC 2017*. <https://doi.org/10.1109/PVSC.2017.8366322>
- Höök, M., & Tang, X. (2013). Depletion of fossil fuels and anthropogenic climate change-A review. *Energy Policy*. <https://doi.org/10.1016/j.enpol.2012.10.046>
- Iqbal, M. (1983). Extraterrestrial Solar Irradiation. In M. Iqbal (Ed.), *An Introduction to Solar Radiation* (pp. 59–84). <https://doi.org/10.1016/b978-0-12-373750-2.50009-4>
- Janssen, G. J. M., Van Aken, B. B., Carr, A. J., & Mewe, A. A. (2015). Outdoor Performance of Bifacial Modules by Measurements and Modelling. *Energy Procedia*. <https://doi.org/10.1016/j.egypro.2015.07.051>
- Jerez, S., Montavez, J. P., Jimenez-Guerrero, P., Gomez-Navarro, J. J., Lorente-Plazas, R., & Zorita, E. (2013). A multi-physics ensemble of present-day climate regional simulations over the Iberian Peninsula. *Climate Dynamics*, *40*(11), 3023–3046. <https://doi.org/10.1007/s00382-012-1539-1>
- Kalogirou, S. A. (2014). Solar Energy Engineering: Processes and Systems: Second Edition. In *Solar Energy Engineering: Processes and Systems: Second Edition*. <https://doi.org/10.1016/C2011-0-07038-2>
- Karaveli, A. B. (2018). Development of the Algorithm of Solar Turnkey: Solar Electricity Software for Turkey. <https://doi.org/10.13140/RG.2.2.28371.63529>
- King, D. L., Boyson, W. E., & Kratochvill, J. A. (2004). *SANDIA REPORT Photovoltaic Array Performance Model*. (December), 43. Retrieved from

<http://www.ntis.gov/help/ordermethods.asp?loc=7-4-0#online>

- Kopecek, R., Veschetti, Y., Gerritsen, E., Schneider, A., Comparotto, C., Mihailechi, V. D., ... Libal, J. (2015). Bifaciality: One Small Step for Technology, One Giant Leap for kWh Cost Reduction. *Photovoltaics International*.
- Letin, V. A., Kagan, M. B., Nadorov, V. P., & Zajavlin, V. R. (2000). Bifacial solar arrays of Russian space crafts. *Conference Record of the IEEE Photovoltaic Specialists Conference*. <https://doi.org/10.1109/PVSC.2000.916071>
- Lo, C. K., Lim, Y. S., & Rahman, F. A. (2015). New integrated simulation tool for the optimum design of bifacial solar panel with reflectors on a specific site. *Renewable Energy*. <https://doi.org/10.1016/j.renene.2015.03.047>
- Louw, J. A., & Rix, A. J. (2019). Irradiance modelling for bi-facial PV modules using the ray tracing technique. *Proceedings - 2019 Southern African Universities Power Engineering Conference/Robotics and Mechatronics/Pattern Recognition Association of South Africa, SAUPEC/RobMech/PRASA 2019*. <https://doi.org/10.1109/RoboMech.2019.8704817>
- Luque, A., Ruiz, J. M., Cuevas, A., Eguren, J., & Gomez-Agost, J. . (1980). DOUBLE-SIDED $n^+ - p - n^+$ SOLAR CELL FOR BIFACIAL CONCENTRATION. *Solar Cells: Their Science, Technology, Applications and Economics*, 2(2), 151–166. [https://doi.org/10.1016/0379-6787\(80\)90007-1](https://doi.org/10.1016/0379-6787(80)90007-1)
- Luque, Antonio, & Hegedus, S. (2011). Handbook of Photovoltaic Science and Engineering. In *Handbook of Photovoltaic Science and Engineering*. <https://doi.org/10.1002/9780470974704>
- Marion, B., MacAlpine, S., Deline, C., Asgharzadeh, A., Toor, F., Riley, D., ... Hansen, C. (2018). *A Practical Irradiance Model for Bifacial PV Modules*. <https://doi.org/10.1109/pvsc.2017.8366263>

- Masters, G. M. (2013). Renewable and efficient electric power systems. In *Choice Reviews Online* (Vol. 42). <https://doi.org/10.5860/choice.42-3448>
- Menicucci, D. F., & Fernandez, J. P. (1989). User ' s Manual for PVFORM: A Photovoltaic System Shulation Program For Stand-Alone and Grid-interactive Applications. *Sandia Report*, (October), 94. Retrieved from http://infoserve.sandia.gov/sand_doc/1985/850376.pdf
- Meulenberg, A., Allison, J. F., & Arndt, R. A. (n.d.). Thin n-i-p silicon solar cell. *14th IEEE Photovoltaic Specialists Conference*, 161–165. San Diego.
- Mori, H. (1966). *Patent No. 3.278.811*. Retrieved from <https://patents.google.com/patent/US3278811%0Ahttps://patentimages.storage.googleapis.com/9a/61/9e/14fb2dc4fdf4c1/US3278811.pdf>
- Neamen, D. A. (2006). Semiconductor Physics and Devices Basic Principles. In *Materials Today*. [https://doi.org/10.1016/S1369-7021\(06\)71498-5](https://doi.org/10.1016/S1369-7021(06)71498-5)
- Peel, M. C., Finlayson, B. L., & McMahon, T. A. (2007). Updated world map of the Köppen-Geiger climate classification. *Hydrology and Earth System Sciences*. <https://doi.org/10.5194/hess-11-1633-2007>
- Perez, R., Ineichen, P., Seals, R., Michalsky, J., & Stewart, R. (1990). Modeling daylight availability and irradiance components from direct and global irradiance. *Solar Energy*. [https://doi.org/10.1016/0038-092X\(90\)90055-H](https://doi.org/10.1016/0038-092X(90)90055-H)
- Photovoltaik-Institut Berlin PI. (2019). *Bifacial. Ready for Mass Deployment*. 1–9.
- Pierret, R. F. (1996). Semiconductor Device Fundamentals. *New York*. <https://doi.org/10.1007/BF00198606>
- Savage, N., Agnew, P., Davis, L., Ordonez, C., Thorpe, R., Johnson, C., ... Dalvi, M. (2012). Air quality modelling using the Met Office Unified Model (AQUUM OS24-26): Model description and initial evaluation. *Geoscientific Model Development Discussions*, 5, 3131–3182. <https://doi.org/10.5194/gmdd-5-3131-2012>

- Saw, M. H., Khoo, Y. S., Singh, J. P., & Wang, Y. (2017). Enhancing optical performance of bifacial PV modules. *Energy Procedia*. <https://doi.org/10.1016/j.egypro.2017.09.285>
- Shoukry, I., Berrian, D., Libal, J., & Haffner, F. (2018). Simulation models for energy yield prediction of bifacial systems. In *Bifacial Photovoltaics: Technology, applications and economics*. https://doi.org/10.1049/pbpo107e_ch4
- Shoukry, I., Libal, J., Kopecek, R., Wefringhaus, E., & Werner, J. (2016). Modelling of Bifacial Gain for Stand-alone and in-field Installed Bifacial PV Modules. *Energy Procedia*. <https://doi.org/10.1016/j.egypro.2016.07.025>
- Soria, B., Gerritsen, E., Lefillastre, P., & Broquin, J. E. (2016). A study of the annual performance of bifacial photovoltaic modules in the case of vertical facade integration. *Energy Science and Engineering*. <https://doi.org/10.1002/ese3.103>
- Spencer, J. W. (1971). Fourier Series Representation of the Position of the Sun. *Search*, 2(5), 172.
- Strobl, G., Kasper, C., Rasch, K. D., & Roy, K. (1985). Bifacial Space Silicon Solar Cell. *Conference Record of the IEEE Photovoltaic Specialists Conference, 1*, 454–457.
- Sun, X., Khan, M. R., Deline, C., & Alam, M. A. (2018). Optimization and performance of bifacial solar modules: A global perspective. *Applied Energy*. <https://doi.org/10.1016/j.apenergy.2017.12.041>
- Taylor, M. H., Losch, M., Wenzel, M., & Schröter, J. (2013). On the sensitivity of field reconstruction and prediction using empirical orthogonal functions derived from Gappy data. *Journal of Climate*. <https://doi.org/10.1175/JCLI-D-13-00089.1>
- Valdivia, C. E., Li, C. T., Russell, A., Haysom, J. E., Li, R., Lekx, D., ... Schriemer, H. P. (2018). *Bifacial Photovoltaic Module Energy Yield Calculation and*

Analysis. <https://doi.org/10.1109/pvsc.2017.8366206>

- Van Aken, B. B., Okel, L. A. G., Liu, J., Luxembourg, S. L., & van Roosmalen, J. A. M. (2016). White Bifacial Modules – Improved STC Performance Combined with Bifacial Energy Yield. *32nd European Photovoltaic Solar Energy Conference and Exhibition*, 42–47. <https://doi.org/10.4229/EUPVSEC20162016-1BO.12.2>
- Wang, S., Wilkie, O., Lam, J., Steeman, R., Zhang, W., Khoo, K. S., Rostan, H. (2015a). Bifacial Photovoltaic Systems Energy Yield Modelling. *Energy Procedia*. <https://doi.org/10.1016/j.egypro.2015.07.060>
- Wang, S., Wilkie, O., Lam, J., Steeman, R., Zhang, W., Khoo, K. S., Rostan, H. (2015b). Bifacial Photovoltaic Systems Energy Yield Modelling. *Energy Procedia*, 77, 428–433. <https://doi.org/10.1016/j.egypro.2015.07.060>
- Wasfi, M. (2011). Solar Energy and Photovoltaic Systems. *Solar Energy and Photovoltaic Systems*.
- Willmott, C. J., Matsuura, K., & Robeson, S. M. (2009). Ambiguities inherent in sums-of-squares-based error statistics. *Atmospheric Environment*. <https://doi.org/10.1016/j.atmosenv.2008.10.005>
- Yusufoglu, Ufuk A., Pletzer, T. M., Koduvelikulathu, L. J., Comparotto, C., Kopecek, R., & Kurz, H. (2015). Analysis of the annual performance of bifacial modules and optimization methods. *IEEE Journal of Photovoltaics*. <https://doi.org/10.1109/JPHOTOV.2014.2364406>
- Yusufoglu, Ufuk Alper, Lee, T. H., Pletzer, T. M., Halm, A., Koduvelikulathu, L. J., Comparotto, C., ... Kurz, H. (2014). Simulation of energy production by bifacial modules with revision of ground reflection. *Energy Procedia*. <https://doi.org/10.1016/j.egypro.2014.08.111>